nature ecology & evolution

ARTICLES

https://doi.org/10.1038/s41559-021-01435-x

Check for updates

Balancing selection maintains hyper-divergent haplotypes in *Caenorhabditis elegans*

Daehan Lee[1,10,14], Stefan Zdraljevic[1,2,11,12,14], Lewis Stevens[1,14], Ye Wang[1,13], Robyn E. Tanny[1], Timothy A. Crombie[1], Daniel E. Cook[1], Amy K. Webster[3,4], Rojin Chirakar[3], L. Ryan Baugh[3,5], Mark G. Sterken[6], Christian Braendle[7], Marie-Anne Félix[8], Matthew V. Rockman[9] and Erik C. Andersen[1]✉

Across diverse taxa, selfing species have evolved independently from outcrossing species thousands of times. The transition from outcrossing to selfing decreases the effective population size, effective recombination rate and heterozygosity within a species. These changes lead to a reduction in genetic diversity, and therefore adaptive potential, by intensifying the effects of random genetic drift and linked selection. Within the nematode genus *Caenorhabditis*, selfing has evolved at least three times, and all three species, including the model organism *Caenorhabditis elegans*, show substantially reduced genetic diversity relative to outcrossing species. Selfing and outcrossing *Caenorhabditis* species are often found in the same niches, but we still do not know how selfing species with limited genetic diversity can adapt to these environments. Here, we examine the whole-genome sequences from 609 wild *C. elegans* strains isolated worldwide and show that genetic variation is concentrated in punctuated hyper-divergent regions that cover 20% of the *C. elegans* reference genome. These regions are enriched in environmental response genes that mediate sensory perception, pathogen response and xenobiotic stress response. Population genomic evidence suggests that genetic diversity in these regions has been maintained by long-term balancing selection. Using long-read genome assemblies for 15 wild strains, we show that hyper-divergent haplotypes contain unique sets of genes and show levels of divergence comparable to levels found between *Caenorhabditis* species that diverged millions of years ago. These results provide an example of how species can avoid the evolutionary dead end associated with selfing.

Across the tree of life, selfing species have evolved independently from outcrossing species thousands of times[1,2]. This reproductive mode transition has profound effects on the evolutionary processes that shape the genome. For example, selfing reduces the effective population size (by a factor of two)[3] and the efficacy of recombination, leading to stronger effects of linked selection (selective sweeps of beneficial mutations or background selection against deleterious mutations)[4,5]. Furthermore, because a single selfing individual can seed an entire population, founder effects are expected to be more severe[6,7]. Together, these factors lead to a substantial reduction in the genetic diversity in selfing species[8]. This reduced diversity is expected to limit the ability of these lineages to adapt to new environments and could ultimately lead to their extinction, known as the evolutionary dead end hypothesis, potentially explaining why most selfing lineages are evolutionarily young[9].

Outcrossing nematode species have some of the highest levels of diversity across all eukaryotes, but the species that predominantly reproduce by self-fertilization have at least an order of magnitude less variation than their outcrossing relatives[10–12]. In the nematode genus *Caenorhabditis*, self-fertilization has evolved independently at least three times, including in the model organism *Caenorhabditis elegans*[13]. Although *C. elegans* is capable of outcrossing, genetic evidence suggests that the selfing rate of this species is 99%[14–16]. As expected in species with high selfing rates, linked selection strongly influences genome-wide patterns of genetic diversity. Four of the six *C. elegans* chromosomes show evidence of large-scale selective sweeps that have reduced diversity across large portions of the worldwide population[10]. Despite limited genetic diversity, *C. elegans* has colonized diverse environmental niches throughout the world[17]. Perhaps counterintuitively, strains whose genomes have been subject to the selective sweeps are found much more frequently and exhibit a wider ecological range than strains that have avoided the selective sweeps[10,18]. This observation, and evidence that the selective sweeps probably occurred within the past 200–300 years, led to the hypothesis that the swept haplotype might harbour adaptive alleles that are favourable in human-associated habitats[10]. This hypothesis is further supported by the observation that divergent strains are typically isolated from natural habitats that are more isolated from human activity[18].

Balancing selection can maintain adaptive genetic variation for long periods of time against evolutionary forces that constantly

[1]Department of Molecular Biosciences, Northwestern University, Evanston, IL, USA. [2]Interdisciplinary Biological Sciences Program, Northwestern University, Evanston, IL, USA. [3]Department of Biology, Duke University, Durham, NC, USA. [4]University Program in Genetics and Genomics, Duke University, Durham, NC, USA. [5]Center for Genomic and Computational Biology, Duke University, Durham, NC, USA. [6]Laboratory of Nematology, Wageningen University and Research, Wageningen, the Netherlands. [7]Université Côte d'Azur, CNRS, Inserm, IBV, France, Nice, France. [8]Institut de Biologie de l'Ecole Normale Supérieure, Centre National de la Recherche Scientifique, INSERM, École Normale Supérieure, Paris Sciences et Lettres, Paris, France. [9]Center for Genomics and Systems Biology, Department of Biology, New York University, New York, NY, USA. [10]Present address: Center for Integrative Genomics, University of Lausanne, Lausanne, Switzerland. [11]Present address: Department of Human Genetics, University of California, Los Angeles, CA, USA. [12]Present address: Howard Hughes Medical Institute, University of California, Los Angeles, CA, USA. [13]Present address: Sichuan Key Laboratory of Conservation Biology on Endangered Wildlife, Chengdu Research Base of Giant Panda Breeding, Chengdu, People's Republic of China. [14]These authors contributed equally: Daehan Lee, Stefan Zdraljevic, Lewis Stevens. ✉e-mail: erik.andersen@northwestern.edu

reduce genetic diversity (for example, genetic drift and background selection). Although genome-wide scans for signatures of long-term balancing selection often have limited abilities to detect balanced loci, a handful of examples have been identified, predominantly in selfing species[19–22]. For example, recent scans in the *Capsella* genus have identified polymorphisms in immune response loci that have been maintained since the divergence of selfing and outcrossing species[23]. Additionally, long-term balancing selection in immune response genes have also been found in flies[24] and humans[25]. Long-term balancing selection increases the coalescent times of neutral sites that are tightly linked to the selected alleles[26], causing balanced haplotypes to accumulate higher-than-average levels of variation over time. It is hypothesized that the evolutionary forces that reduce genetic variation in selfing species have the potential to increase this genomic footprint of loci under balancing selection[27,28]. Intriguingly, genomic loci under long-term balancing selection have also been characterized in *C. elegans*[29–31], and previous comparisons between the genome of the laboratory reference strain N2 and a de novo genome assembly of a divergent Hawaiian strain (CB4856) led to the discovery of punctuated regions of extremely high divergence[32,33].

Here, by examining the whole-genome sequences of 609 wild *C. elegans* strains isolated across the world, we discovered previously uncharacterized levels and patterns of genetic diversity in this species. Our analysis of short- and long-read sequence data led to the identification of 366 distinct hyper-divergent regions that span approximately 20% of the *C. elegans* reference genome. These regions are enriched for genes that mediate environmental responses, contain genes that are not present in the reference N2 genome, and are often shared among many wild strains, suggesting that genetic diversity in hyper-divergent regions might be maintained to enable the species to thrive in diverse environments. Furthermore, the hyper-divergent haplotypes within these regions have levels of divergence comparable to that found between *Caenorhabditis* species that diverged millions of years ago. Finally, by characterizing hyper-divergent regions of another selfing species, *Caenorhabditis briggsae*, we show that punctuated regions of hyper-divergence are probably a common feature in the genomes of selfing *Caenorhabditis* species.

Results

Global distribution of *C. elegans* genetic diversity. To explore the genetic diversity in *C. elegans*, we examined whole-genome sequence data from 609 wild *C. elegans* strains isolated from six continents and several oceanic islands, including 103 wild strains that have not been studied previously (Fig. 1a and Supplementary Table 1). We identified 328 distinct genome-wide genotypes (henceforth, referred to as isotypes) (Methods)[15,34]. The majority of wild strains (368 strains) were classified into isotypes in which each strain in the isotype was sampled from the same location, which is consistent with previous observations that local habitats frequently consist of clonal populations[15,34]. However, we discovered 14 isotypes that were sampled from locations at least 50 km apart (Supplementary Fig. 1a and Supplementary Table 2), suggesting that individuals can migrate long distances in the wild. We used species-wide variant data (2,431,645 single-nucleotide variants (SNVs) and 845,797 insertion and deletion variants of ≤50 base pairs (bp) in length) to identify the most highly divergent isotypes, which were isolated exclusively from a Pacific region that encompasses the Hawaiian islands, New Zealand and the Pacific coast of the United States (Fig. 1a,b and Supplementary Fig. 1b–e).

To further characterize the geographic population structure within *C. elegans*, we performed principal component analysis (PCA)[35] and found that most of the isotypes (326 isotypes) could be classified into three genetically distinct groups (global, Hawaiian and Pacific groups) (Fig. 1c–f and Supplementary Fig. 2). The largest global group includes 93.9% (308) of all isotypes from six continents and oceanic islands (Fig. 1e). The Hawaiian group consists of eight isotypes from the Big Island of Hawaii (Fig. 1d) and the Pacific group includes ten isotypes from Hawaii, California and New Zealand (Fig. 1f). This population structure is consistent with previous studies in which Hawaiian strains were shown to harbour higher genetic diversity than the rest of the worldwide population[18]. Hawaii is the only location where the isotypes of all three groups have been found. For example, the Big Island harbours 25 isotypes from all three groups, whereas all 167 European isotypes belong only to the global group (Fig. 1d–f). Furthermore, the two most divergent isotypes, XZ1516 and ECA701, which do not belong to any of the three groups, were sampled from Kauai, the oldest sampled Hawaiian island (Fig. 1c). The remarkable genetic diversity sampled from the Hawaiian islands suggests that *C. elegans* could have originated from the Pacific region[10,18]. The current geographic location with the most divergent strains might not reflect the origin of the species because worldwide sampling is uneven and some sites, including Asia, have not been sampled extensively. Therefore, *C. elegans* could have originated elsewhere and spread throughout the Pacific region.

Next, we attempted to further subdivide the global group using PCA. This group includes all non-Pacific isotypes and the majority of isotypes from the Pacific Rim. Although we found weak genetic differentiation of global isotypes isolated from Hawaii, North America and Atlantic locations from the rest of the global isotypes, this group was not further clustered into distinct genetic groups (Supplementary Fig. 2 and 3). Additionally, the global group could not be separated into distinct geographic locations because many genetically similar isotypes have been sampled from different continents. By characterizing genomic regions predicted to be identical by descent, we found that the previously reported chromosome-scale selective sweeps[10] contribute substantially to the genetic similarity we observed among geographically distant isotypes (Extended Data Fig. 1 and Supplementary Fig. 3). For example, a large haplotype block on the centre of chromosome V is shared by isotypes from six continents (Africa, Asia, Australia, Europe, North America and South America) (Extended Data Fig. 1). In addition to the Hawaiian isotypes that were reported to have avoided these selective sweeps[18], we found that the genomes of isotypes from Atlantic islands (for example, the Azores, Madeira and São Tomé), in contrast with continental isotypes, show less evidence of the globally distributed haplotype that swept through the species (Extended Data Fig. 1 and Supplementary Table 3).

Discovery of species-wide hyper-divergent genomic regions. Previous studies have shown that genetic variation is distributed non-randomly across each of the five *C. elegans* autosomes, with the chromosome arms harbouring more genetic variation than the chromosome centres[10]. This distribution is shaped by higher recombination rates on chromosome arms than centres, which influences the effects of background selection[36–38]. Consistent with previous studies[10], we observed 2.2-fold higher levels of nucleotide diversity (π) on chromosome arms compared with centres (Welch's t-test; $P < 2.2 \times 10^{-16}$) (Extended Data Fig. 2). Furthermore, we found that variation is concentrated in punctuated regions of extremely high diversity that are marked by a higher-than-average density of small variants and large genomic spans where short sequence reads fail to align to the N2 reference genome (Fig. 2a and Supplementary Fig. 4).

We sought to characterize the species- and genome-wide distributions of these regions (henceforth, referred to as hyper-divergent regions). To facilitate the accurate identification of these hyper-divergent regions across the *C. elegans* species, we generated high-quality genome assemblies using long-read sequencing data for 14 isotypes that span the species-wide diversity (Methods and

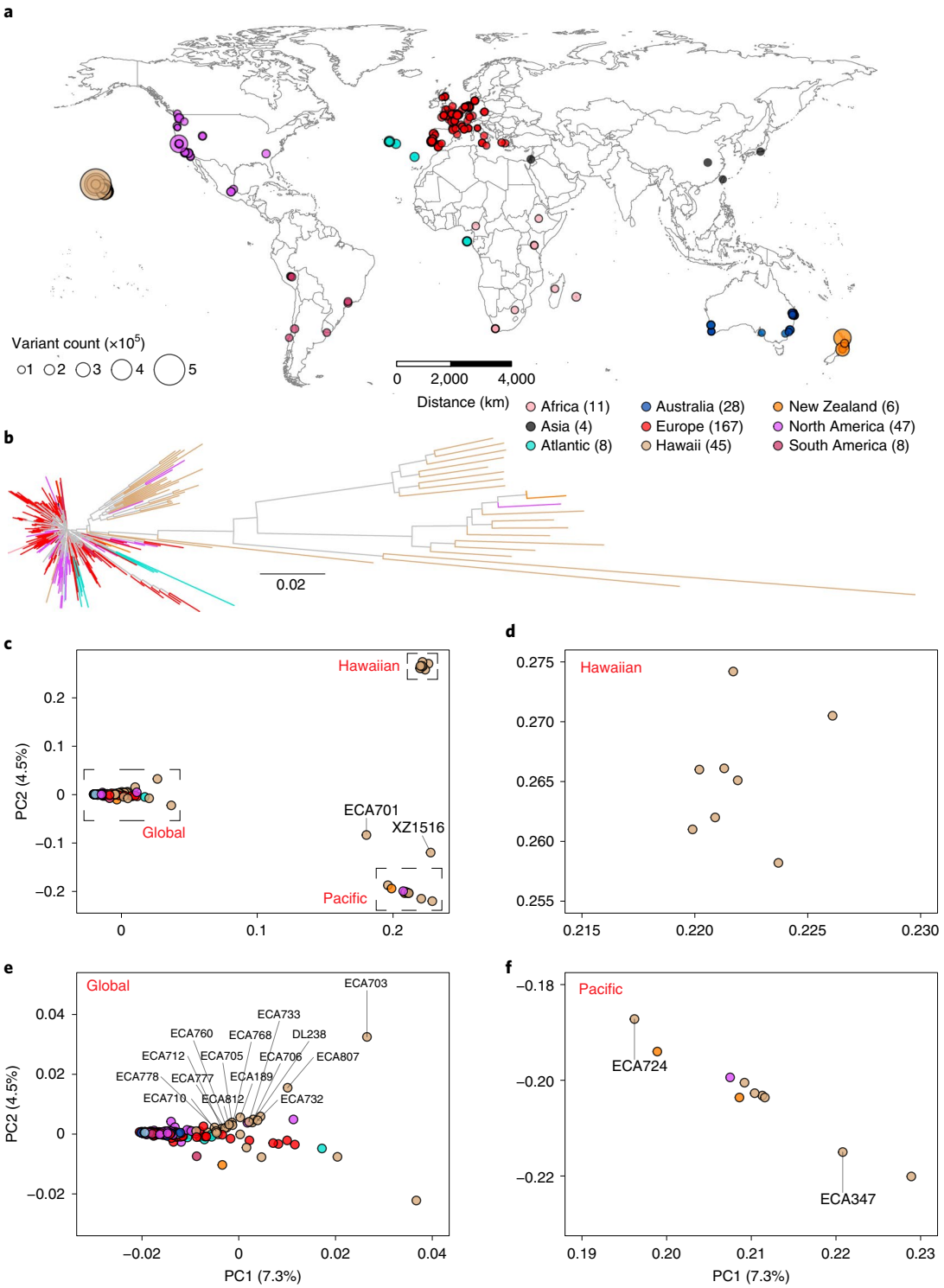

Fig. 1 | Genetically divergent wild *C. elegans* strains isolated from the Pacific region. a, Global distribution of 324 isotypes. Each circle corresponds to one of the 324 isotypes and is coloured by geographic origin. Four isotypes for which we do not have geographic information are not shown. The size of each circle corresponds to the number of non-reference homozygous alleles. The number of isotypes from each geographic origin is labelled in parentheses. **b**, Neighbour-joining tree of 328 *C. elegans* isotypes generated from 963,027 biallelic segregating sites. The tips for four isotypes with unknown geographic origins are coloured grey and the other 324 isotypes are coloured by geographic origin, as in **a**. **c**, Plots of the 328 isotypes according to their values for each of the two significant axes of variation, as determined by PCA of the genotype covariances. Each point is one of the 328 isotypes, which are coloured by their geographic origin as in **b**. Two divergent isotypes, XZ1516 and ECA701, are labelled. **d**–**f**, Magnified plots of the Hawaiian (**d**), global (**e**) and Pacific (**f**) groups shown in **c**. In **c**, **e** and **f**, isotypes from the Big Island of Hawaii are labelled. All isotypes in the Hawaiian group were isolated from the Big Island of Hawaii.

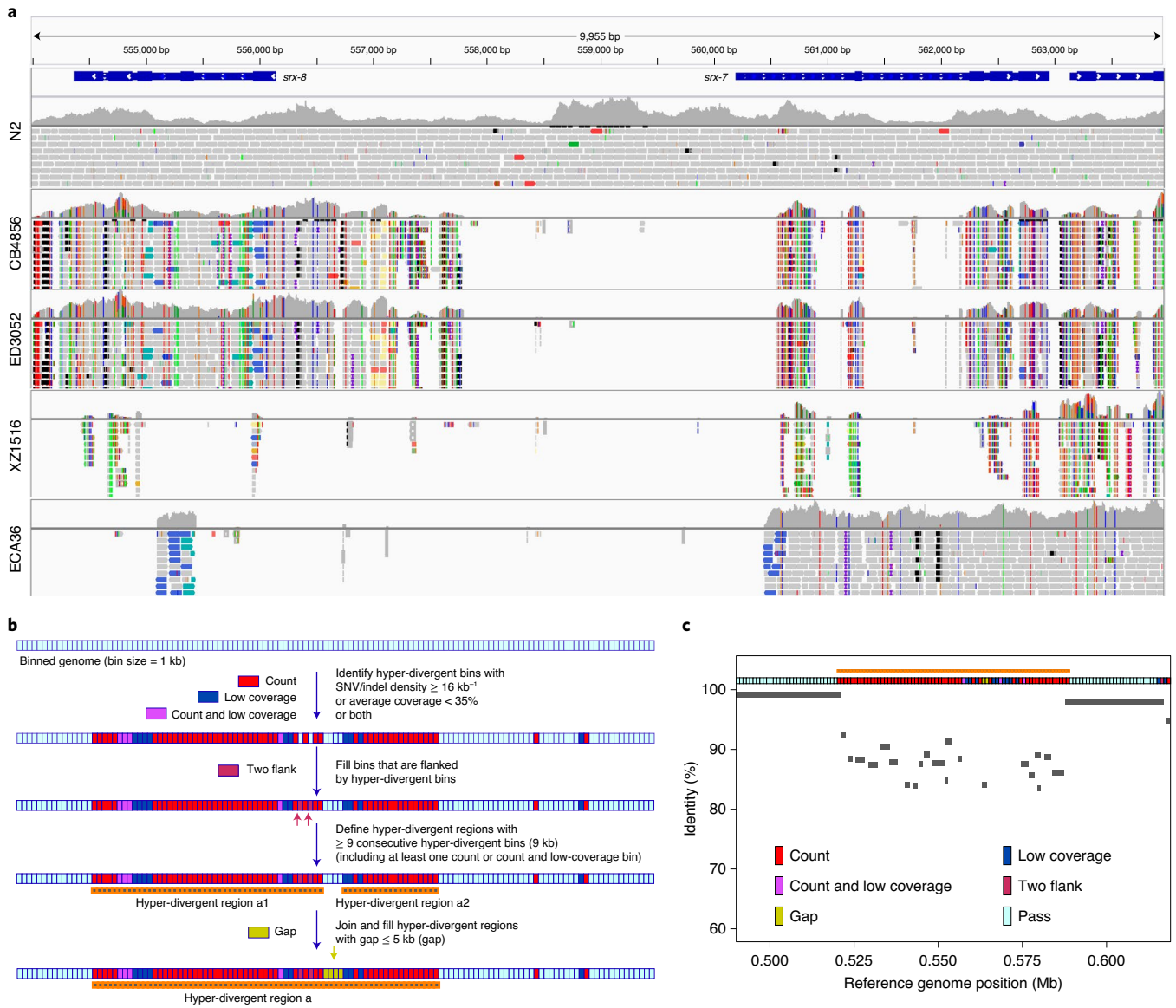

Fig. 2 | Characterization of hyper-divergent regions at the isotype level. a, Short-read alignments from five isotypes (N2, CB4856, ED3052, XZ1516 and ECA36) to the N2 reference genome (WS245) for a region of chromosome V (V:554,000–564,000). Genes (*srx-7* and *srx-8*) in the interval are shown at the top. For each isotype, the top panel shows the coverage of genomic positions and the bottom panel shows aligned short reads at genomic positions (grey, normal reads; red, reads with putative deletion; blue, reads with putative insertion; navy and turquoise, reads with putative inversion; green, reads with putative duplication or translocation). The coloured vertical lines indicate mismatched bases at the position. **b**, Workflow for the characterization of hyper-divergent regions at the isotype level (see Methods). **c**, An example plot showing the short-read-based characterization of a hyper-divergent region and the percentage sequence identity from a long-read alignment. The orange horizontal line shows a hyper-divergent region (V:520,000–589,000) in the locus (V:490,000–619,000) of CB4856 that was classified using this approach. The multi-coloured horizontal rectangle shows classifications of genomic bins in the locus. Grey bars correspond to the alignments from CB4856 long-read sequences to the N2 reference genome (WS245). Identities of alignments are shown on the *y* axis.

Supplementary Table 4). First, we aligned these assemblies, along with a previously published long-read assembly of the Hawaiian isotype CB4856[33], to the N2 reference genome. Next, we used these alignments to classify hyper-divergent regions across a range of parameter values (for example, alignment coverage and sequence divergence). We performed a similar parameter search procedure using short-read alignments of these 15 isotypes and identified a set of short-read parameters that maximized the overlap between long- and short-read hyper-divergent classification (Methods and Extended Data Fig. 3). This analysis identified the optimal parameters to classify hyper-divergent regions as at least nine consecutive 1-kilobase (kb) bins that have one or both of the following criteria: (1) ≥16 SNVs/indels; or (2) <35% read depth to the genome-wide average (Fig. 2b,c). To validate our approach, we compared the hyper-divergent regions we identified in the CB4856 isotype with what was previously reported in this isotype (2.8 megabases (Mb))[32] and found that we detected a similar number and extent of these regions (3.2 Mb). Finally, we applied these optimized short-read hyper-divergent region classification parameters to the entire set of 327 non-reference isotypes.

Across all isotypes, we identified 366 non-overlapping genomic regions that are hyper-divergent from the reference isotype N2

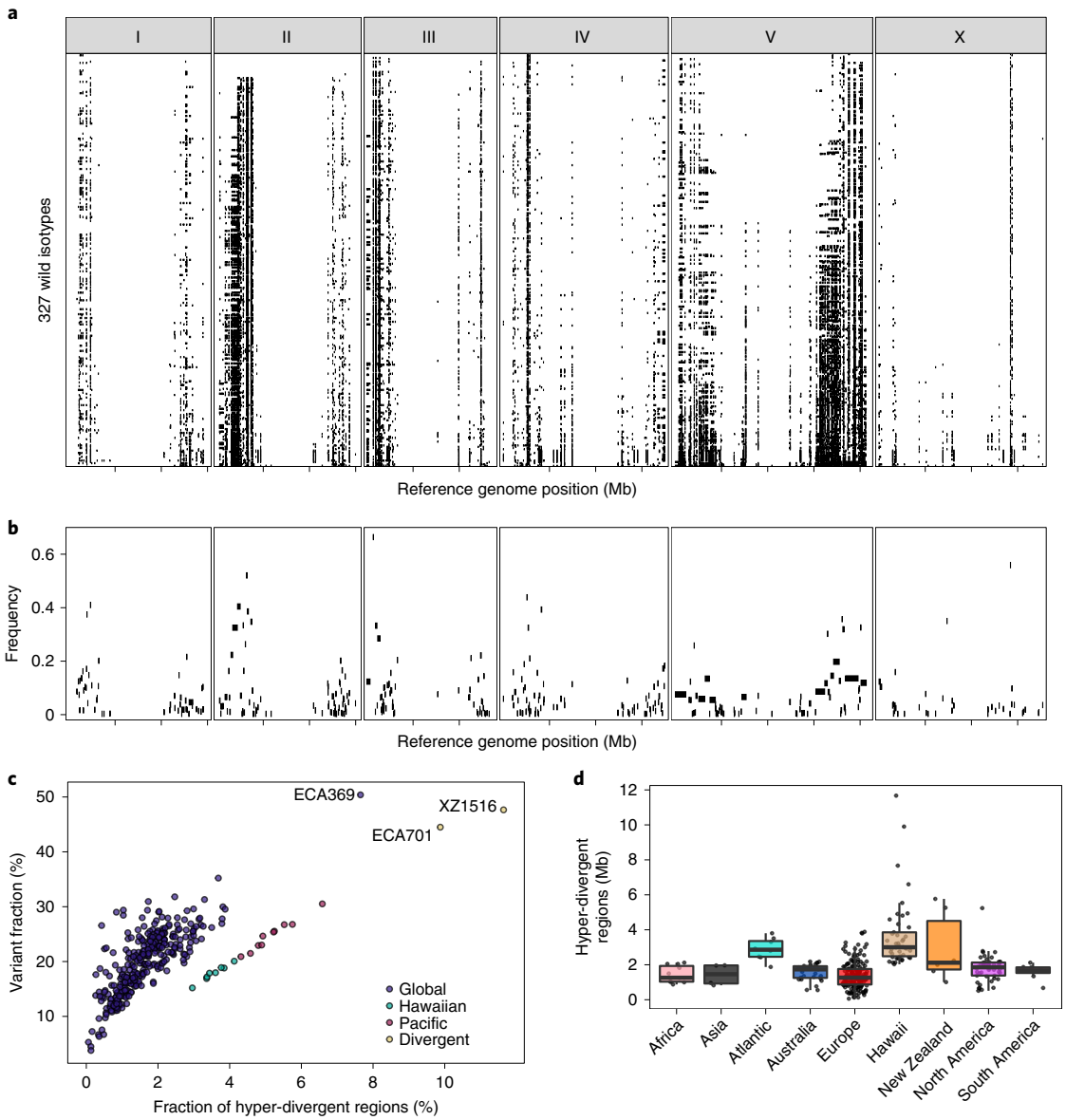

Fig. 3 | Punctuated hyper-divergent genomic regions are widespread across the *C. elegans* species. a, Genome-wide distribution of hyper-divergent regions across 327 non-reference wild *C. elegans* isotypes. Each row represents one of the 327 isotypes, ordered by the total amount of genome covered by hyper-divergent regions (black). **b**, Species-wide frequencies of hyper-divergent calls for 366 species-wide hyper-divergent regions (see Methods). Each rectangle corresponds to a block of species-wide hyper-divergent regions. The average frequencies of hyper-divergent calls across 1-kb bins in each block across 327 non-reference isotypes are shown on the *y* axis. In **a** and **b**, the genomic position using the N2 reference is plotted on the *x* axis and each tick represents 5 Mb of the chromosome. **c**, Scatter plot of the extent of the N2 reference genome that is hyper-divergent in each isotype (*x* axis) and the fraction of total variants in hyper-divergent regions of 327 non-reference isotypes (*y* axis). Each point corresponds to one of the 327 isotypes and is coloured by the genetic grouping (Fig. 1c). The three isotypes with the largest genome-wide extents of hyper-divergent regions are labelled. **d**, Tukey box plots of the total amount of genome covered by hyper-divergent regions, with data points plotted behind. Isotypes are grouped by geographic origin. Each point corresponds to one of the 324 isotypes with a known geographic origin. The extent of the N2 reference genome that is hyper-divergent in each isotype is shown on the *y* axis. The horizontal line in the middle of each box is the median; box edges denote the 25th and 75th quantiles of the data; and whiskers represent 1.5× the interquartile range.

in at least one isotype (Fig. 3a,b, Supplementary Table 5 and Supplementary Data 1). These regions range in size from 9 kb to 1.35 Mb (mean = 56 kb; median = 19 kb) (Supplementary Fig. 5) and cover approximately 20% of the N2 reference genome (20.5 Mb). The majority of these regions (69%) are found on autosomal arms and have 10.3-fold higher variant (SNV/indel) densities than the non-divergent autosomal arm regions (16.6-fold more than the genome-wide average) (Supplementary Table 6 and Extended Data Fig. 4). Although variant counts are probably underestimated because short sequencing reads often fail to align to the reference genome in hyper-divergent regions, we note that the level of genetic diversity in these regions is similar to the level of genetic diversity reported in outcrossing *Caenorhabditis* species[39,40]. Across all non-reference isotypes, we found substantial differences in the extent of the genome that was classified as hyper-divergent (0.06–11.6% of the genome) (Fig. 3c,d). The genome of the most divergent

isotype (XZ1516) contains a striking 11.7 Mb of hyper-divergent regions. In general, smaller fractions of the genomes of global group isotypes were classified as hyper-divergent, which reflects that these isotypes are more closely related to the reference N2 isotype (Fig. 3c). A notable exception to this trend is the global group isotypes that were isolated from Atlantic islands, which have, on average, a larger extent of their genome classified as hyper-divergent than the rest of the global group (Fig. 3d). On average, 20.2% of the variation in a typical isotype is found in hyper-divergent regions that span 1.9% of the reference genome (Fig. 3c and Supplementary Table 3).

Maintenance of hyper-divergent haplotypes. The species-wide distribution of hyper-divergent regions revealed that many non-reference isotypes are often hyper-divergent at the same regions of the N2 reference genome (Figs. 3a,b and Fig. 4a). We found that these regions range from being divergent in a single isotype to divergent in 280 isotypes (85%). Interestingly, we found that SNVs in hyper-divergent regions have a lower rate of linkage disequilibrium decay than SNVs within non-divergent regions on the autosomal arms (Fig. 4b), suggesting that these regions are inherited as large haplotype blocks. We performed genome-wide scans using commonly used statistics (Tajima's D and standardized β) to identify regions under long-term balancing selection[21,23,30], which could explain the presence of hyper-divergent haplotype blocks that are shared by a substantial fraction of isotypes[26]. We found that signatures of long-term balancing selection are concentrated in genomic regions that are frequently classified as hyper-divergent across the species (Fig. 4c–f). We note that estimates for Tajima's D and β are probably biased towards lower values in hyper-divergent regions because short reads often fail to align in these regions (Extended Data Fig. 5), which causes genetic diversity to be underestimated. Together, these results suggest that hyper-divergent haplotypes, which are frequently shared among many isotypes, have been maintained in the *C. elegans* species by long-term balancing selection.

Balancing selection can maintain genetic diversity that contributes to the adaptive potential of a population in the presence of environmental heterogeneity[41]. To investigate whether hyper-divergent regions are functionally enriched for genes that enable *C. elegans* to thrive in diverse habitats, we performed gene set enrichment analysis using two complementary approaches (Methods and Supplementary Data 2 and 3). Sensory perception and xenobiotic stress response were among the most significantly enriched gene classes (Fig. 4g, Extended Data Fig. 6 and Supplementary Fig. 6). For example, we found that 54.9% (802/1,461) of seven-transmembrane receptor class genes (for example, G protein-coupled receptors (GPCRs)) are located in hyper-divergent regions. In addition to GPCRs, 48.2% (124/257) of genes that encode for C-type lectins, 53% (317/598) of the E3 ligase genes and 86.8% (33/38) of the *pals* genes, which are involved in responses to diverse pathogens[31,42–45] are found in hyper-divergent regions (Supplementary Fig. 7 and Supplementary Data 2). In agreement with these enrichment results, we found that 66.8% (131/196) and 65.4% (85/130) of genes that are differentially expressed in the reference N2 isotype upon exposure to the natural pathogens *Nematocida parisii*[46] or Orsay virus[47], respectively, are located in these regions[48] (Supplementary Fig. 8). Furthermore, we found that genes in hyper-divergent regions are more strongly induced than genes in non-divergent regions of the genome (Welch's t-test; $P = 0.00606$ for *N. parisii* and $P = 0.0002226$ for Orsay virus) (Supplementary Fig. 8). Notably, we found that hyper-divergent regions overlap with previously characterized genomic loci underlying natural variation in responses to the *C. elegans* pathogens *N. parisii*[49] and Orsay virus[50], as well as responses to pathogens not found to be associated with *C. elegans* in nature[51]. These results suggest that high levels of variation in hyper-divergent regions probably facilitate diverse pathogen responses across the species.

Hyper-divergent haplotypes contain potentially ancient genetic diversity. A common feature of the hyper-divergent regions is that short-read sequencing coverage is lower than the average genome-wide coverage (47% less coverage on average), suggesting that divergence in these regions is too high for accurate alignment of short reads to the reference genome. Therefore, we took advantage of the 15 long-read genome assemblies to assess the content of these hyper-divergent regions. Strikingly, we found that these regions contain multiple hyper-divergent haplotypes that contain unique sets of genes and alleles that have substantially diverged at the amino acid level. For example, a hyper-divergent region on chromosome II (II:3,667,179–3,701,405 in the N2 reference genome) contains three distinct hyper-divergent haplotypes across the 16 isotypes for which we have high-quality assemblies (Fig. 5a). In this region, the reference isotype (N2) shares a haplotype with three isotypes and contains 11 protein-coding genes, including six encoding GPCRs (*srx-97*, *srx-98*, *srx-101*, *srx-102*, *srx-104* and *srx-105*). A second haplotype is shared among 11 isotypes and contains 20 protein-coding genes, including ten that are not conserved in the reference haplotype. The third haplotype is found only in a single isotype (DL238) and contains 17 protein-coding genes, including six that are not present in the reference haplotype. Of the 16 genes that are not conserved across the three haplotypes, 13 have clear homology to *srx-101*, *F40H7.12* or *F19B10.10* (all found within this region in the reference haplotype) and three genes have homology to genes elsewhere in the genome, suggesting they have originated via duplication and diversification of existing genes, rather than de novo gene birth (Fig. 5a and Supplementary Data 4). For those genes that are conserved across all three haplotypes, alleles in different hyper-divergent haplotypes commonly show <95% amino acid identity (for example, *F19B10.10* has an average between-haplotype identity of 88.3%, while *srx-97*, which lies outside the divergent

Fig. 4 | Balancing selection has maintained hyper-divergent haplotypes enriched in environmental response genes. a, Tukey box plots of the total amount of genome covered by common hyper-divergent regions, with data points plotted behind. Isotypes are grouped by their geographic origin. Each point corresponds to one of the 327 non-reference isotypes. The horizontal line in the middle of each box is the median; box edges denote the 25th and 75th quantiles of the data; and whiskers represent 1.5× the interquartile range. **b**, Linkage disequilibrium decay in non-divergent and hyper-divergent regions in autosomal arms. Note that 99.9% confidence intervals are represented around each smoothed line (generalized additive model fitting) as grey bands, but these are not visible because of the narrow range of the intervals. Distances between SNVs are shown on the x axis and linkage disequilibrium statistical values (r^2) are shown on the y axis. **c**, Genome-wide pattern of Tajima's D. Each point represents a non-overlapping 1-kb genomic region and is coloured by its divergent classification (non-divergent region (grey), rare (<1%; orange), intermediate (≥1 and <5%; blue) or common (≥5%; green) hyper-divergent region). **d**, Genome-wide pattern of standardized beta statistics (β_{std}). Each dot corresponds to the value for a particular variant, coloured by its location, as in **c**. In **c** and **d**, the reference genome position is plotted on the x axis and each tick represents 5 Mb of the chromosome. **e**,**f**, Stacked bar plots showing fractions of genomic bins (1 kb) for Tajima's D (**e**) and fractions of variants for β_{std} (**f**). Genomic bins and variants are grouped and coloured by their location as in **c**. The numbers in the bar plots represent counts of genomic bins (**e**) or variants (**f**). **g**, Gene set enrichment for autosomal arm regions (squares) and hyper-divergent regions (circles). Bonferroni-corrected significance values for gene set enrichment are shown on the x axis. The sizes of the squares and circles correspond to the fold enrichment of the annotation and the colours of the squares and circles correspond to the gene counts of the annotation. The blue line shows the Bonferroni-corrected significance threshold (corrected P value = 0.05).

region, has an average between-haplotype identity of 98.4%; Fig. 5b). The relationships inferred for this region using short-read SNV data were consistent with those relationships inferred using the long-read assemblies (Fig. 5a), allowing us to infer the haplotype composition of all non-reference isotypes for this region (Methods and Extended Data Fig. 7a). We found that a total of 59 isotypes contain the reference haplotype, 267 isotypes contain the second divergent haplotype and one other isotype shares the DL238 haplotype.

In other regions of the genome, we found different numbers of hyper-divergent haplotypes across the 16 isotypes. For example, at the *peel-1 zeel-1* incompatibility locus on chromosome I (I:2,318,291–2,381,851 in the N2 reference genome), which was previously characterized to be maintained by long-term

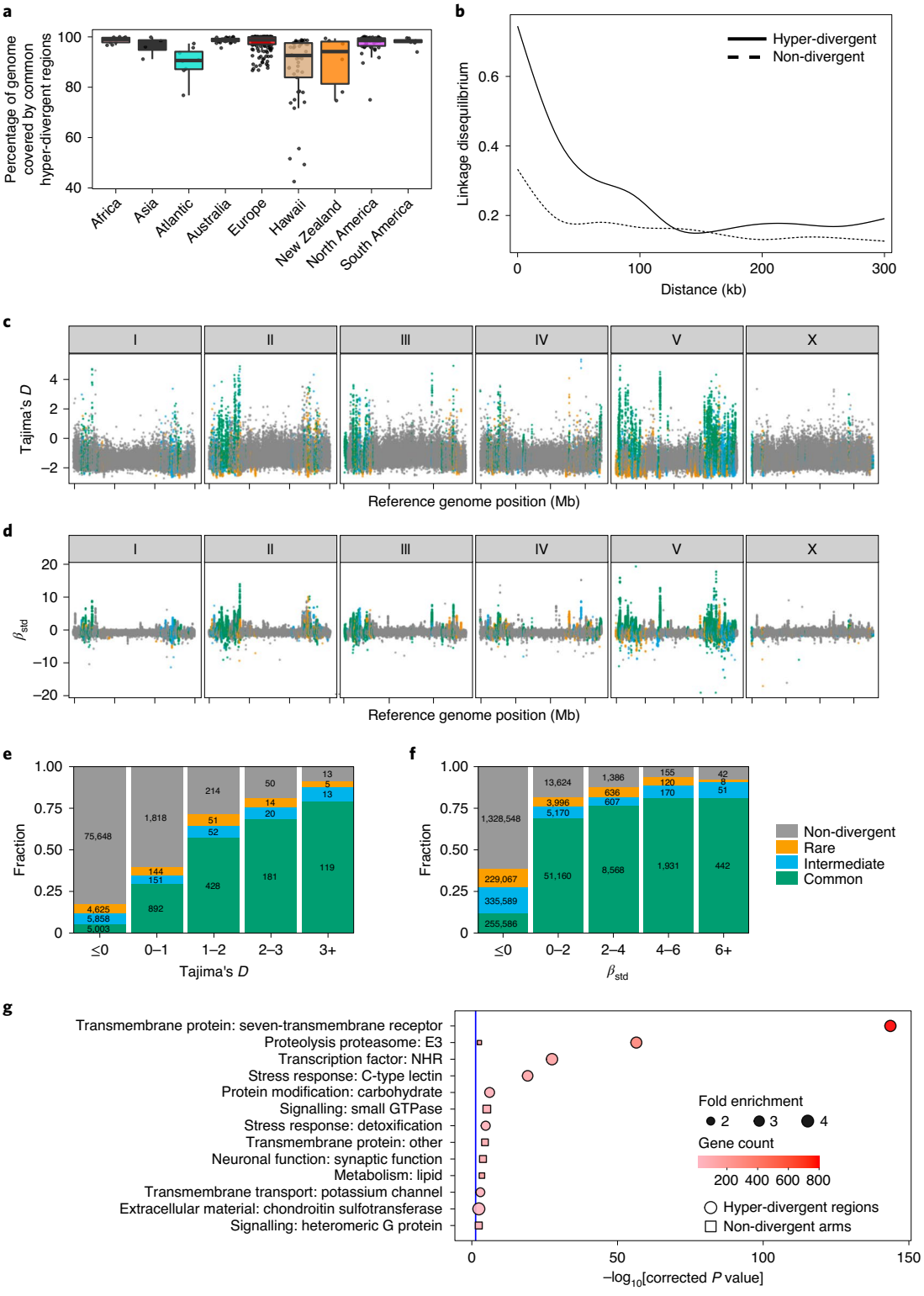

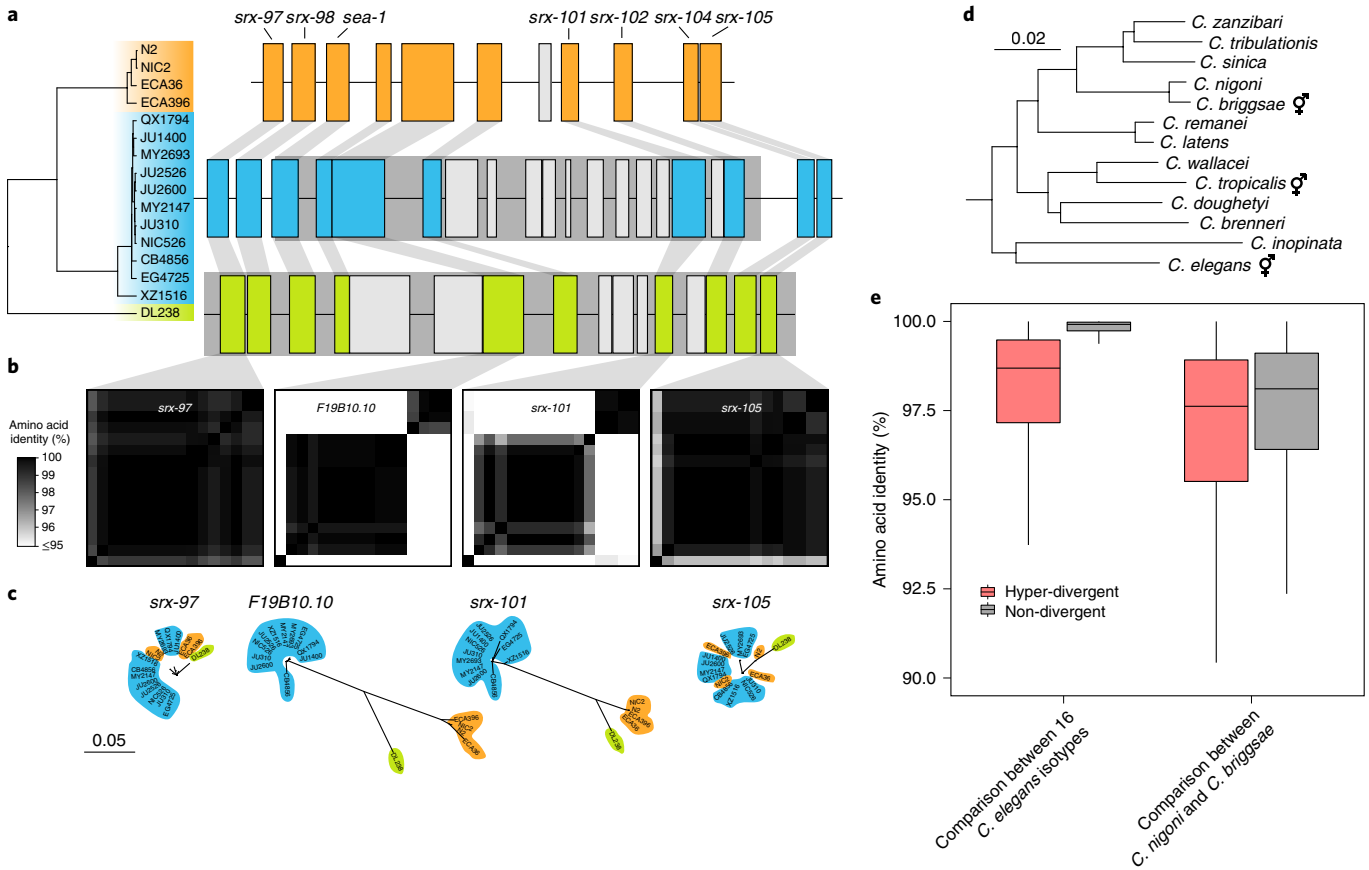

Fig. 5 | Hyper-divergent haplotypes contain ancient genetic diversity. a, Protein-coding gene contents of three hyper-divergent haplotypes in a region on the left arm of chromosome II (II:3,667,179–3,701,405 of the N2 reference genome). The tree was inferred using SNVs and coloured by the inferred haplotypes. For each distinct haplotype, we chose a single isotype as a haplotype representative (orange haplotype, N2; blue haplotype, CB4856; green haplotype, DL238) and predicted protein-coding genes using both protein-based alignments and ab initio approaches (see Methods). Protein-coding genes are shown as boxes. Those genes that are conserved in all haplotypes are coloured based on their haplotype and those genes that are not are coloured light grey. Dark grey boxes behind loci indicate the coordinates of the hyper-divergent regions. Genes with locus names in N2 are highlighted. **b**, Heatmaps showing amino acid identities for the alleles of four loci (*srx-97*, *F19B10.10*, *srx-101* and *srx-105*). The percentage identity was calculated using alignments of protein sequences from all 16 isotypes. The heatmaps are ordered by the SNV tree shown in **a**. **c**, Maximum-likelihood gene trees of four loci (*srx-97*, *F19B10.10*, *srx-101* and *srx-105*) inferred using amino acid alignments. All trees are plotted on the same scale (scale shown, in amino acid substitutions per site). The isotype names are coloured by their haplotype. **d**, *Caenorhabditis* phylogeny showing relationships within the *Elegans* subgroup[118]. Species that reproduce via self-fertilization are indicated. The scale is in amino acid substitutions per site. **e**, Tukey box plots showing the amino acid identities of 8,741 genes that are single copy and present in all 16 *C. elegans* isotypes, *C. briggsae* and *C. nigoni*. The identities of alleles and their orthologues are shown separately for hyper-divergent and non-divergent regions.

balancing selection[29], we found two distinct hyper-divergent haplotypes across the 16 isotypes (Extended Data Fig. 8). The reference haplotype contains the *peel-1* and *zeel-1* toxin-antidote genes, which are absent in the alternative haplotype (Extended Data Fig. 8). As expected under long-term balancing selection, genes that are linked to the *peel-1 zeel-1* locus show elevated sequence divergence. For example, the gene immediately adjacent to *zeel-1*, *ugt-31*, has an average between-haplotype identity of 95.7%, but *mcm-4*, which lies outside the divergent region, has an average between-haplotype identity of 99.9% (Extended Data Fig. 8b). In another region on the right arm of chromosome V (V:20,193,463–20,267,244 in the N2 reference genome) that contains three F-box genes (*fbxa-114*, *fbxa-113* and *fbxb-59*), we found between six and seven hyper-divergent haplotypes, each with their own unique complement of genes (Extended Data Fig. 9 and Supplementary Data 4). Strikingly, the six hyper-divergent alleles of the F-box gene *fbxb-59* all show <95% identity to each other (Extended Data Fig. 9b). Consistent with our hypothesis of long-term balancing selection, the sharing of haplotypes in all three regions presented here does not reflect the species-wide relationships (Fig. 5c and Extended Data Figs. 7, 8c and 9c). Instead, divergent isotypes from the Hawaiian and Pacific groups often share haplotypes with the global group isotypes, suggesting that these haplotypes have been maintained since the last common ancestor of all sampled *C. elegans* isotypes.

To contextualize the high divergence we observe in hyper-divergent regions, we compared the level of divergence between hyper-divergent haplotypes with that observed between closely related *Caenorhabditis* species. As *C. elegans* lacks a closely related sister species (Fig. 5d), we compared the amino acid identities of *C. elegans* hyper-divergent alleles with the divergence between their orthologues in *C. briggsae* and *C. nigoni*, a closely related pair of species that are believed to have diverged from each other approximately 3.5 million years ago[52]. Notably, the average identity between hyper-divergent alleles within *C. elegans* is comparable to the divergence of their orthologues between *C. briggsae* and *C. nigoni* (mean identities in hyper-divergent regions of 97.7 and 96.4%, respectively, compared with mean identities in non-divergent regions of 99.6 and 97.0%, respectively; Fig. 5e). Taken together, these results suggest

that hyper-divergent haplotypes might have diverged millions of years ago.

Hyper-divergent regions are common features in the genomes of selfing *Caenorhabditis* species. Selfing has evolved at least three times independently in the *Caenorhabditis* genus and is the main reproductive mode for *C. elegans*, *C. briggsae* and *C. tropicalis*[16,53] (Fig. 5d). We hypothesized that long-term balancing selection might have maintained punctuated hyper-divergent haplotypes in other selfing species. We used our short-read classification approach to identify hyper-divergent regions in the genomes of 35 wild *C. briggsae* strains[52]. In agreement with our hypothesis, we found that hyper-divergent regions are widespread in the genomes of wild *C. briggsae* strains (Extended Data Fig. 10 and Methods). Moreover, we found that the same regions are divergent in strains from the tropical *C. briggsae* clade and divergent strains from other clades[52]. Therefore, it is likely that the same evolutionary processes that have maintained genetic diversity in *C. elegans* have also shaped the genome of *C. briggsae*, and that hyper-divergent regions are common features in the genomes of selfing *Caenorhabditis* species.

Discussion

Theory and empirical evidence show that predominantly selfing species have less genetic diversity than obligately outcrossing species[38]. It follows that reduced levels of genetic diversity in selfing species would limit the adaptive potential and range of ecological niches that the species can inhabit[54]. However, *C. elegans* and other selfing *Caenorhabditis* species are globally distributed, found in diverse habitats and often share niches with outcrossing nematode species[16,55]. We provide evidence that remarkable genetic diversity in hyper-divergent regions probably contributes to the distribution of *C. elegans* across diverse niches. We found that these genomic regions are significantly enriched for genes that modulate responses to bacteria, competitors and pathogens in wild habitats[17], including GPCRs, C-type lectins and the *pals* gene family. Previous studies have functionally characterized hyper-divergent alleles of such genes within these regions that have profound impacts on *C. elegans* physiology and ecology. For example, distinct density-dependent foraging strategies have been shown to be mediated by hyper-divergent alleles of two neighbouring genes (*srx-43* and *srx-44*) that encode for GPCRs[30,56]. A quantitative trait locus on chromosome III that affects pheromone-induced developmental plasticity[57] is another example of a hyper-divergent region associated with an ecologically relevant *C. elegans* phenotype. Furthermore, the enrichment of immune response genes that we observed in hyper-divergent regions suggests that these regions might harbour variation that enables *C. elegans* to survive various pathogenic threats. In support of this hypothesis, previous studies have shown substantial genetic and phenotypic variation in response to the co-evolved fungal and viral pathogens *N. parisii*[49] and Orsay virus[50], respectively. Four genomic regions were originally identified to affect *C. elegans* susceptibility to *N. parisii*, all of which overlap with hyper-divergent regions we identified. Subsequent studies showed that the *pals* genes mediate responses to *N. parisii* and the Orsay virus[31,42–45], of which 86.8% (33/38) are located in hyper-divergent regions. The hyper-divergent regions we present here also include other loci previously found to underlie natural resistance to starvation[58] and toxic bacterial metabolites[59], as well as genetic incompatibilities in the species[29,60]. However, the loci discussed here only represent a handful of the 366 distinct hyper-divergent regions we identified, suggesting that we still have much to learn about the role of these regions in *C. elegans* ecology and physiology.

The punctuated nature of the hyper-divergent haplotypes can be explained by the predominantly selfing lifestyle of *C. elegans*. Selfing leads to a reduction in the effective recombination rate and therefore increases linkage disequilibrium, which increases the overall footprint of balancing selection[27,28]. Furthermore, long-term selfing causes an overall reduction in genome-wide diversity[8], making the high genetic diversity in balanced regions of the genome more pronounced. Given that the outcrossing *Caenorhabditis* species also inhabit diverse niches, just as *C. elegans* does, long-term balancing selection for environmental response genes could have occurred and shaped hyper-divergent haplotypes in those species as well. However, hyper-divergent haplotypes under long-term balancing selection in outcrossing species are expected to be more difficult to identify because they are likely to be smaller and less pronounced from the background of much higher genetic diversity.

Our findings highlight the limitations of short-read reference-based mapping approaches for characterizing variation in genetically diverse species. Using de novo genome assemblies generated from long-read data, we have shown that hyper-divergent haplotypes contain levels of genetic variation that are substantially underestimated using short-read-based approaches, including genes that are not present in the reference genome and alleles that are highly diverged at the amino acid level. A similar observation was recently reported in soybean[61], where thousands of dispensable genes and large structural variants were discovered using genome assemblies generated using long-read data. Exploiting these new sequencing technologies will be critical if we are to fully capture patterns of genetic variation in *C. elegans* and other species.

The origin of hyper-divergent haplotypes in *C. elegans* remains elusive. We hypothesize that ancient balancing selection and adaptive introgression could be two possible sources of hyper-divergent haplotypes. Hyper-divergent haplotypes could represent ancestral genetic diversity that has been maintained by balancing selection since the evolution of selfing in *C. elegans*, which is believed to have occurred in the past 4 million years[62]. The amino acid divergence among *C. elegans* hyper-divergent haplotypes is similar to the divergence between *C. briggsae* and *C. nigoni*, two species that diverged approximately 3.5 million years ago[52], suggesting that these haplotypes could have been maintained for millions of years. Moreover, outcrossing *Caenorhabditis* species typically have extremely high levels of genetic diversity[11,12]. Assuming the outcrossing ancestor of *C. elegans* was similarly diverse, these hyper-divergent regions might represent the last remnants of ancestral genetic diversity that has otherwise been lost because of the long-term effects of selfing. Similar observations have been reported in the *Capsella* genus, where the selfing species, *Capsella rubella*, shares variants with its outcrossing sister species *Capsella grandiflora*[63]. These *trans*-specific polymorphisms are predominantly found at loci involved in immune response[23], which match our findings in *C. elegans*. Alternatively, hyper-divergent haplotypes could have been introgressed from other species. Introgression was recently shown to explain the existence of large, divergent haplotypes that underlie ecotypic adaptation in sunflowers[64] and are characterized in other species[65]. Niche sharing of different *Caenorhabditis* species is often observed in natural habitats[16,18,55], suggesting that hybridization with closely related species could have occurred in the *C. elegans* lineage. Because *C. elegans* and its closest known relative, *C. inopinata*, are estimated to have diverged 10.5 million years ago[66], it is not possible to distinguish between retained ancestral polymorphism and relatively recent introgression by identifying *trans*-specific polymorphisms. However, the presence of up to seven *C. elegans* hyper-divergent haplotypes at a single locus suggests that introgression is unlikely to be an exclusive source of hyper-divergent haplotypes. Notably, we characterized a similar pattern of punctuated hyper-divergent regions in *C. briggsae*, which is a selfing species with a closely related outcrossing species, *C. nigoni*. As similar population-wide variant data become available for *C. briggsae*, it might be possible to test whether the patterns of divergence are consistent with introgression, retained ancestral genetic diversity or both.

Regardless of their origin, the existence of these regions in *C. elegans* has important implications for how we understand the genetic and genomic consequences of selfing. It has been proposed that the evolution of selfing represents an evolutionary dead end, whereby the reduction in genetic diversity, and therefore the adaptive potential, of a species will eventually lead to extinction[9]. However, our findings suggest that it is possible to avoid this fate by maintaining a substantial fraction of the ancestral or introgressed genetic diversity at key regions of the genome.

Methods

Strains. Nematodes were reared at 20 °C using *Escherichia coli* bacteria (strain OP50) grown on modified nematode growth medium (NGMA)[67] containing 1% agar and 0.7% agarose to prevent animals from burrowing. All 609 wild *C. elegans* strains are available from the *Caenorhabditis elegans* Natural Diversity Resource (CeNDR)[68] and strain information can be found in the accompanying metadata (Supplementary Table 1).

Sequencing and isotype characterization. *Sequencing.* To extract DNA, we transferred nematodes from two 10-cm NGMA plates spotted with OP50 into a 15-ml conical tube by washing with 10 ml M9. We then used gravity to settle animals in a conical tube, removed the supernatant and added 10 ml fresh M9. We repeated this wash method three times over the course of 1 h to serially dilute the *E. coli* in the M9 and allow the animals time to purge ingested *E. coli*. Genomic DNA was isolated from 100–300 µl nematode pellets using the Blood & Tissue DNA isolation kit (69506; Qiagen) following established protocols[69]. The DNA concentration was determined for each sample with the Qubit dsDNA Broad Range Assay Kit (Q32850; Invitrogen). The DNA samples were then submitted to the Duke Sequencing and Genomic Technologies Shared Resource per their requirements. The Illumina library construction and sequencing were performed at Duke University using KAPA HyperPrep kits (Kapa Biosystems) and the Illumina NovaSeq 6000 platform (paired-end 150-bp reads). The raw sequencing reads for strains used in this project are available from the National Center for Biotechnology Information (NCBI) Sequence Read Archive (project PRJNA549503).

Isotype characterization. Raw sequencing reads from 609 wild strains were trimmed using Trimmomatic (version 0.36)[70] to remove low-quality bases and adapter sequences. Following trimming, we called SNVs using BCFtools (version 1.9)[71] and the following filters: depth ≥ 3; mapping quality > 40; variant quality > 30; allelic depth/number of high-quality bases ratio > 0.5. We classified two or more strains as the same isotype if they had the same call at 99.9% of all sites called across the full panel of wild strains. If a strain did not meet this criterion, we considered it a unique isotype. Newly assigned isotypes were added to CeNDR[68].

Pacific Biosciences continuous long-read sequencing. To extract DNA, we transferred nematodes from 12 10-cm NGMA plates spotted with OP50 into a 50-ml conical tube by washing with 30 ml M9. We then used gravity to settle the animals for 1.5 h, removed the supernatant and added 15 ml fresh M9. We allowed the nematodes to settle for 1 h, removed the supernatant and transferred the nematodes to a microfuge tube using a Pasteur pettle. We settled the animals for an additional 1 h and any supernatant was removed. We stored pellets at −80 °C before DNA extraction. Genomic DNA was isolated from 400–500 µl nematode pellets using the MagAttract HMW DNA kit (67563; Qiagen). The DNA concentration was determined for each sample with the Qubit dsDNA Broad Range Assay Kit (Q32850; Invitrogen). The DNA samples were submitted to the Duke Sequencing and Genomic Technologies Shared Resource for library construction and sequencing using the Pacific Biosciences Sequel platform. Quality control was performed with the Qubit dsDNA Broad Range Assay Kit and Agilent TapeStation. Some samples had 30- to 50-kb fragment sizes; a 15-kb cut-off was used for size selection of these samples during library preparation. A 20-kb cut-off was used for the other samples. The raw sequencing reads for strains used in this project are available from the NCBI Sequence Read Archive (project PRJNA692613).

Sequence alignments and variant calling. After isotypes were assigned, we used BWA (version 0.7.17-r1188)[72,73] to align trimmed sequence data for distinct isotypes to the N2 reference genome (WS245)[74]. Variants were called using GATK4 (version 4.1.0)[75]. First, genomic variant call format files (gVCFs) were generated for each isotype using the HaplotypeCaller function in GATK4 with the parameters --max-genotype-count = 3000 and --max-alternate-alleles = 100, using the WS245 N2 reference genome. Next, individual isotype gVCFs were merged using the MergeVcfs function in GATK4 and imported to a genomics database using the GenomicsDBImport function. Genotyping of the gVCFs was performed using the GenotypeGVCFs function in GATK4 with the parameter --use-new-qual-calculator. The 328-isotype-cohort VCF was annotated using SnpEff[76] and an annotation database that was built with the WS261 gene annotations[76]. Following VCF annotation, we applied soft filters (QualByDepth (QD) < 5.0; StrandOddsRatio (SOR) > 5.0; variant quality < 30.0; ReadPosRankSum < −5.0; FisherStrand (FS) > 50.0; depth < 5) to the VCF variants using the VariantFiltration function in GATK4. We applied a final isotype-specific soft filter called dv_dp using the bcftools filter function, which required the alternative allele depth to be at least 50% of the total read depth for an individual isotype. All variant sites that failed to meet the variant-level filter criteria were removed from the soft-filtered VCF, and all isotype-level variants that did not meet the dv_dp criteria were set to missing. Finally, we removed sites that had >5% missing genotype data or where >10% of samples were called heterozygous.

Genetic relatedness. *Similarity analysis.* Using BCFtools (version 1.9) with the command filter -i N_MISSING = 0, we filtered the high-quality VCF file and generated a VCF file (complete-site VCF) containing 963,027 biallelic SNVs that are genotyped for all 328 *C. elegans* isotypes. We used the vcf2phylip.py script[77] to convert the complete-site VCF file to the PHYLIP format. The distance matrix and unrooted neighbour-joining tree were made from this PHYLIP file using dist.ml and the NJ function using the phangorn (version 2.5.5) R package[78]. The tree was visualized using the ggtree (version 1.16.6) R package[79].

PCA. The smartpca executable from EIGENSOFT (version 6.1.4)[35,80] was used to perform PCA. We performed analysis with the complete-site VCF with or without removing outlier isotypes to analyse the population structure with highly genetically divergent isotypes. When analysing the population without removing outlier isotypes, we used the following parameters: altnormstyle: NO; numoutevec: 50; and familynames: NO. When analysing the population with outlier isotype removal, we set maximum number of outlier removal iterations to 15.

Population genomic analyses. *Haplotype analysis.* We determined the identity by descent of genome segments using IBDSeq (version r1206)[81] run on the complete-site VCF with the following parameters: minalleles = 0.01; r2window = 1,500; ibdtrim = 0; r2max = 0.3 for genome-wide haplotype analysis. Identity-by-descent segments were then used to infer haplotype structure among isotypes, as described previously[10]. We defined the most common haplotype in each of chromosomes I, IV, V and X, of which the species-wide average fraction of the most common haplotype is >30%, as the swept haplotype for each chromosome. We then retained the swept haplotypes within isotypes that passed the following per-chromosome filters: total length > 1 Mb; total length/maximum population-wide swept haplotype length > 0.03.

Population genetics. We only considered biallelic SNVs to calculate population genomic statistics. Tajima's *D*, Watterson's θ and π were all calculated using scikit-allel[82]. Each of these statistics was calculated for the same non-overlapping 1,000-bp windows as hyper-divergent regions (as described below). We calculated the standardized $\beta^{(1)}$ (refs. [83,84]) using the BetaScan.py script by providing Watterson's θ estimates with the -thetaMap flag. Default window parameters surrounding each marker were used (±500 bp from the focal marker).

Linkage disequilibrium decay. We filtered the complete-site VCF file using BCFtools (version 1.9) with the command view -q 0.05:minor and generated a VCF file (MAF-05 VCF) containing 123,830 SNVs of which minor allele frequencies are ≥5%. Then, we selected 41,368 SNVs on autosomal arms (MAF-05-autoarm VCF) and split the MAF-05-autoarm VCF (by the location of SNVs) into MAF-05-autoarm-div VCF (with 17,419 SNVs within the hyper-divergent autosomal arm) and MAF-05-autoarm-nondiv VCF (with 23,949 SNVs within the non-divergent autosomal arms). We analysed linkage disequilibrium decay by running PopLDdecay (version 3.31)[85] on both MAF-05-autoarm-div VCF and MAF-05-autoarm-nondiv VCF with the default parameters (MaxDist = 300; Het = 0.88; Miss = 0.25).

Long-read genome assembly. We extracted PacBio reads in FASTQ format from the subread BAM files using the PacBio bam2fastx tool (version 1.3.0; available at https://github.com/PacificBiosciences/bam2fastx). For each of the 14 isotypes, we assembled the PacBio reads using three genome assemblers: wtdbg2 (version 0.0; using the parameters -x sq -g 102 m)[86], flye (version 2.7; using the parameters --pacbio-raw -g 102 m)[87] and Canu (version 1.9; using the parameters genomeSize = 102 m -pacbio-raw)[88]. For each assembly, we assessed the biological completeness using BUSCO[89] (version 4.0.6; using the options -l nematoda_odb10 -m genome) and the contiguity by calculating a range of numerical metrics using scaffold_stats.pl (available at https://github.com/sujaikumar/assemblage). We selected the Canu assemblies as our final assemblies because they had both high contiguity and high biological completeness. To correct sequencing errors that remained in the Canu assemblies, we aligned short-read Illumina data for each isotype to the corresponding assembly using BWA-MEM[73] (version 0.7.17) and provided the BAM files to Pilon for error correction (version 1.23; using the parameters --changes --fix bases)[90]. To remove assembled contigs that originated from non-target organisms (such as the *E. coli* food source), we screened each assembly using taxon-annotated GC-coverage plots as implemented in BlobTools[91]. Briefly, we aligned the PacBio reads to the assembly using minimap2 (ref. [92]; version 2.17; using the parameters -a -x map-pb) and sorted then indexed the BAM

files using SAMtools[93] (version 1.9). We searched each assembled contig against the NCBI nucleotide database ('nt') using BLASTN[94] (version 2.9.0+; using the parameters -max_target_seqs 1 -max_hsps 1 -evalue 1e-25) and against UniProt Reference Proteomes[95] using Diamond (version 0.9.17; using the parameters blastx --max-target-seqs 1 --sensitive --evalue 1e-25)[96]. We removed contigs that were annotated as being of bacterial origin and that had coverage and a percentage GC that differed from the target genome. Genome assembly metrics are shown in Supplementary Table 4.

Characterization of hyper-divergent regions. To characterize hyper-divergent regions across the *C. elegans* species, we first analysed short- and long-read alignments of 15 isotypes. For all non-overlapping 1-kb windows in the reference *C. elegans* genome, we calculated the number of small variants (SNVs and indels) (variant count) using the coverage subroutine in the BEDtools (version 2.27.1)[97] suite, as well as the average sequencing depth using mosdepth (version 0.2.3)[98]. We converted the coverage values to coverage fraction (average sequencing depth of the window/genome-wide average depth). In parallel, we aligned all 14 long-read assemblies we generated along with a long-read assembly for the Hawaiian isotype CB4856[33] to the N2 reference genome (WS255)[99] using NUCmer (version 3.1) with the parameters --maxgap = 500 --mincluster = 100[100]. Coordinates and identities of the aligned sequences were extracted from the alignment files using the show-coords function with NUCmer. Then, we calculated the average alignment coverage and average alignment identity for each non-overlapping window in the reference genome. Next, we used the long- and short-read alignment datasets to identify the optimal coverage fraction and variant count parameters to apply to the rest of the population for which we did not have long-read sequence data. We tested a wide range of parameters to define hyper-divergent regions from short- and long-read alignments. For the short-read-based approach, we classified each window as hyper-divergent if its variant count was $\geq x$ or its coverage fraction was $<y$% or both. We also classified windows that were flanked by two hyper-divergent windows as hyper-divergent. Then, we clustered contiguous hyper-divergent windows and defined clusters that were ≥9 kb of N2 reference genome length as hyper-divergent regions[32]. For the long-read-based approach, we classified each window as hyper-divergent if its alignment coverage was $<z$% or its alignment coverage was $<w$% or both. We also classified windows that were flanked by hyper-divergent windows as hyper-divergent. Then, we clustered contiguous hyper-divergent windows and defined clusters that were ≥9 kb of the N2 reference genome length as hyper-divergent regions. Because we lacked a true hyper-divergent region dataset to which we could tune our parameters, we identified the set of x, y, z and w values that maximized the overlap between hyper-divergent regions identified by short- and long-read-based approaches (Extended Data Fig. 3). To minimize the false positives that we detected, we manually validated hundreds of regions that were classified as hyper-divergent using IGV[101]. Using this optimization, we selected the optimal short-read classification parameters (variant counts ≥ 16 and coverage fraction < 35%), which we then applied to all 327 non-reference isotypes. With these classification parameters, we identified a hyper-divergent region (3.2 Mb) in CB4856 of similar size to the total size of hyper-divergent regions (2.8 Mb) identified in CB4856 previously[32]. Additionally, we confirmed that the selected parameters did not detect any hyper-divergent region from short-read alignments of the N2 reference strain to its own reference genome. To exclude large deletions that could be classified as hyper-divergent regions, we filtered out hyper-divergent regions without any window with high variant density that exceed the variant count threshold. To classify species-wide hyper-divergent regions, we combined continuous hyper-divergent regions that were identified in individual strains. To compare small variant (SNV/indel) density between hyper-divergent and non-divergent regions for chromosomal centres, arms and tips (Supplementary Table 6), we used previously defined genomic coordinates for the centres, arms and tips of six chromosomes[36]. For bins with no isotype classified as hyper-divergent, we measured the variant density as the average variant density of all 328 isotypes. For bins with at least one isotype classified as hyper-divergent, we measured the variant density as the average variant density of isotypes that were classified as hyper-divergent for each bin. We calculated the percentage of 327 non-reference isotypes that were classified as hyper-divergent (percentage divergence) for each 1-kb bin and classified each bin into one of three frequency groups based on its percent divergence: rare (<1%); intermediate 1–5%; and common (≥5%).

For *C. briggsae*, we performed a sliding window analysis with a 1-kb window size and a 1-kb step size for each of 35 non-reference wild *C. briggsae* genomes[52]. We only used variant counts to classify hyper-divergent regions. Because the *C. briggsae* genome-wide variant density was 1.55 greater than that for *C. elegans*, we used a modified variant count threshold (variant counts ≥ 24). We also classified windows that were flanked by hyper-divergent windows as hyper-divergent.

Gene set enrichment analysis. We analysed the gene set enrichment of hyper-divergent regions using the web-based tool WormCat[102], which contains a near-complete annotation of genes from the *C. elegans* reference strain N2. We also performed a conventional Gene Ontology enrichment analysis using the clusterProfiler (version 3.12.0) R package[103] and org.Ce.eg.db[104]. Because the majority of hyper-divergent regions are found on autosomal arms (Fig. 3a and Supplementary Table 6), we used gene set enrichment on the autosomal arms as a control dataset[36].

Protein-coding gene prediction. To generate ab initio gene predictions for all 14 assemblies and for a previously published long-read assembly for the Hawaiian isotype CB4856[33], we first used RepeatMasker (http://www.repeatmasker.org; version 4.0.9; using the parameter -xsmall) to identify and soft-mask repetitive elements in each genome assembly using a library of known Rhabditida repeats from RepBase[105]. We predicted genes in the masked assemblies using AUGUSTUS (version 3.3.3; using the parameters --genemodel = partial --gff3 = on --species = caenorhabditis --codingseq = on)[106]. We extracted protein sequences and coding sequences from the GFF3 file using the getAnnoFasta.pl script from AUGUSTUS. We assessed the biological completeness of each predicted gene set using BUSCO (version 4.0.6; using the options -l nematoda_odb10 -m proteins), using the longest isoforms of each gene only. Predicted protein-coding gene counts and BUSCO completeness scores are shown in Supplementary Table 4.

Characterizing gene contents of hyper-divergent haplotypes. To characterize and compare the gene contents of hyper-divergent haplotypes, we used OrthoFinder[107] (version 2.3.11; using the parameter -og) to cluster the longest isoform of each protein-coding gene predicted from the genomes of 15 wild isolates and the N2 reference genome (WS270). We initially attempted to use the orthology assignments to identify alleles in the 15 isotypes for each region of interest. However, gene prediction errors were pervasive, with many fused and split gene models, which caused incorrect orthology assignment and/or spurious alignments. To ensure that the differences between hyper-divergent haplotypes were real biological differences and not gene prediction artefacts, we used the AUGUSTUS gene predictions and orthology assignments to identify coordinates of hyper-divergent haplotypes only. For a given region of interest, we identified genes in the reference genome that flanked the hyper-divergent regions and used the orthology assignments to identify the corresponding alleles in all 15 wild isolates. Using the coordinates of these genes, we extracted the sequences of intervening hyper-divergent haplotypes using BEDtools (version 2.29.2; using the parameters getfasta -bed)[97]. To identify genes that were conserved in the reference haplotype, we extracted the longest isoform for each protein-coding gene in this region from the N2 reference gene set and used exonerate[108] (version 2.4.0; using the parameters --model p2g --showvulgar no --showalignment no --showquerygff no --showtargetgff yes) to infer gene models directly for each of the 15 isotypes. To predict genes that were not present in the reference haplotype, we first used BEDtools (version 2.29.2; with the parameter maskfasta) to mask the coordinates of the exonerate-predicted genes with Ns. We then used AUGUSTUS (version 3.3.3; using the parameters --genemodel = partial --gff3 = on --species = caenorhabditis --codingseq = on) to predict genes in the unmasked regions. To remove spurious gene predictions or transposable element loci, we searched the protein sequence of each AUGUSTUS-predicted gene against the N2 reference genome using BLASTP (version 2.9.0+; using the parameters -max_target_seqs 1 -max_hsps 1 -evalue 1e-5) and against the Pfam database[109] using InterProScan (version 5.35–74.0; using the parameters -dp -t p --goterms -appl Pfam -f tsv)[110]. Predicted genes that contained Pfam domains associated with transposable elements, or those genes that lacked sequence similarity to a known *C. elegans* protein sequence and a conserved protein domain were discarded (Supplementary Data 4). The coordinates of all curated predicted protein-coding genes were used to generate gene content plots (Fig. 5a and Extended Data Figs. 8a and 9a) using the ggplot R package[111]. To generate amino acid identity heatmaps and gene trees, we aligned the protein sequences of all conserved genes (those predicted with exonerate) using FSA (version 1.15.9)[112]. We inferred gene trees using IQ-TREE[113] (version 2.0.3), allowing the best-fitting substitution model to be automatically selected for each alignment[114]. Gene trees were visualized using the ggtree R package. We calculated percentage identity matrices from the protein alignments using a custom Python script (available at https://github.com/AndersenLab/Ce-328pop-div). We then generated heatmaps, ordered by the strain relatedness tree inferred for the region, using the ggplot R package[111]. Files containing gene coordinates, protein alignments, gene trees and percentage identity matrices for each characterized region are available at https://github.com/AndersenLab/Ce-328pop-div. To construct dendrograms of hyper-divergent regions, we first converted the hard-filtered VCF to a gds object using the snpgdsVCF2GDS function in the SNPrelate package[115]. Next, we calculated the pairwise identity-by-descent fraction for all strains using the snpgdsIBS function in the SNPrelate R package and performed hierarchical clustering on the matrix using the snpgdsHCluster function in the SNPrelate package. We visualized the strain relatedness using ggtree[79].

Comparing divergence between *C. briggsae* and *C. nigoni*. To compare the divergence between hyper-divergent haplotypes with closely related *Caenorhabditis* species, we downloaded the protein sequences predicted from the genomes of *C. briggsae*[116] and *C. nigoni*[117] from WormBase (WS275). We clustered the longest isoform of each protein-coding gene for both species with the longest isoform of each protein-coding gene in all 16 *C. elegans* isotypes using OrthoFinder (version 2.3.11; using the parameter -og). We identified 8,741 orthogroups containing

protein sequences that were present and single copy in all 18 genomes and aligned their sequences using FSA (version 1.15.9). We calculated a percentage identity matrix for each protein alignment using a custom Python script (available at https://github.com/AndersenLab/Ce-328pop-div). For each of the 15 isotypes, we partitioned the 8,741 genes into those that were classified as being divergent and those that were classified as being non-divergent by our short-read classification approach. We then extracted the percentage identity of the allele of interest and the N2 alleles, and also the percentage identity between the corresponding orthologues in *C. briggsae* and *C. nigoni*. For each gene, we calculated the mean identity between all non-divergent alleles and the corresponding N2 alleles (and between their orthologues in *C. briggsae* and *C. nigoni*) and the mean identity between all hyper-divergent alleles and the corresponding N2 alleles (and between their orthologues in *C. briggsae* and *C. nigoni*).

Reporting Summary. Further information on research design is available in the Nature Research Reporting Summary linked to this article.

Data availability

The raw short-read sequencing reads for the strains used in this project are available from the NCBI Sequence Read Archive (project PRJNA549503). The raw PacBio long-read data, along with the de novo assemblies and gene predictions, are available from the NCBI Sequence Read Archive (project PRJNA692613). Strain information and short-read genomic variation data are available from the CeNDR (www.elegansvariation.org)[68].

Code availability

All datasets and code for generating the figures and tables are available from GitHub (https://github.com/AndersenLab/Ce-328pop-div).

Received: 18 September 2020; Accepted: 26 February 2021;
Published online: 05 April 2021

References

1. Barrett, S. C. H. The evolution of plant sexual diversity. *Nat. Rev. Genet.* **3**, 274–284 (2002).
2. Cutter, A. D. Reproductive transitions in plants and animals: selfing syndrome, sexual selection and speciation. *New Phytol.* **224**, 1080–1094 (2019).
3. Pollak, E. On the theory of partially inbreeding finite populations. I. Partial selfing. *Genetics* **117**, 353–360 (1987).
4. Kaplan, N. L., Hudson, R. R. & Langley, C. H. The 'hitchhiking effect' revisited. *Genetics* **123**, 887–899 (1989).
5. Charlesworth, D. & Charlesworth, B. Quantitative genetics in plants: the effect of the breeding system on genetic variability. *Evolution* **49**, 911–920 (1995).
6. Baker, H. G. Self-compatibility and establishment after 'long-distance' dispersal. *Evolution* **9**, 347–349 (1955).
7. Baker, H. G. Support for Baker's law—as a rule. *Evolution* **21**, 853–856 (1967).
8. Charlesworth, D. & Wright, S. I. Breeding systems and genome evolution. *Curr. Opin. Genet. Dev.* **11**, 685–690 (2001).
9. Stebbins, G. L. Self fertilization and population variability in the higher plants. *Am. Nat.* **91**, 337–354 (1957).
10. Andersen, E. C. et al. Chromosome-scale selective sweeps shape *Caenorhabditis elegans* genomic diversity. *Nat. Genet.* **44**, 285–290 (2012).
11. Cutter, A. D., Baird, S. E. & Charlesworth, D. High nucleotide polymorphism and rapid decay of linkage disequilibrium in wild populations of *Caenorhabditis remanei*. *Genetics* **174**, 901–913 (2006).
12. Dey, A., Chan, C. K. W., Thomas, C. G. & Cutter, A. D. Molecular hyperdiversity defines populations of the nematode *Caenorhabditis brenneri*. *Proc. Natl Acad. Sci. USA* **110**, 11056–11060 (2013).
13. Kiontke, K. et al. *Caenorhabditis* phylogeny predicts convergence of hermaphroditism and extensive intron loss. *Proc. Natl Acad. Sci. USA* **101**, 9003–9008 (2004).
14. Sivasundar, A. & Hey, J. Population genetics of *Caenorhabditis elegans*: the paradox of low polymorphism in a widespread species. *Genetics* **163**, 147–157 (2003).
15. Barrière, A. & Félix, M.-A. High local genetic diversity and low outcrossing rate in *Caenorhabditis elegans* natural populations. *Curr. Biol.* **15**, 1176–1184 (2005).
16. Félix, M.-A. & Duveau, F. Population dynamics and habitat sharing of natural populations of *Caenorhabditis elegans* and *C. briggsae*. *BMC Biol.* **10**, 59 (2012).
17. Schulenburg, H. & Félix, M.-A. The natural biotic environment of *Caenorhabditis elegans*. *Genetics* **206**, 55–86 (2017).
18. Crombie, T. A. et al. Deep sampling of Hawaiian *Caenorhabditis elegans* reveals high genetic diversity and admixture with global populations. *eLife* **8**, e50465 (2019).
19. Andrés, A. M. et al. Targets of balancing selection in the human genome. *Mol. Biol. Evol.* **26**, 2755–2764 (2009).
20. Amambua-Ngwa, A. et al. Population genomic scan for candidate signatures of balancing selection to guide antigen characterization in malaria parasites. *PLoS Genet.* **8**, e1002992 (2012).
21. Siewert, K. M. & Voight, B. F. Detecting long-term balancing selection using allele frequency correlation. *Mol. Biol. Evol.* **34**, 2996–3005 (2017).
22. Wu, Q. et al. Long-term balancing selection contributes to adaptation in *Arabidopsis* and its relatives. *Genome Biol.* **18**, 217 (2017).
23. Koenig, D. et al. Long-term balancing selection drives evolution of immunity genes in *Capsella*. *eLife* **8**, e43606 (2019).
24. Langley, C. H. et al. Genomic variation in natural populations of *Drosophila melanogaster*. *Genetics* **192**, 533–598 (2012).
25. Leffler, E. M. et al. Multiple instances of ancient balancing selection shared between humans and chimpanzees. *Science* **339**, 1578–1582 (2013).
26. Charlesworth, D. Balancing selection and its effects on sequences in nearby genome regions. *PLoS Genet.* **2**, e64 (2006).
27. Nordborg, M., Charlesworth, B. & Charlesworth, D. Increased levels of polymorphism surrounding selectively maintained sites in highly selling species. *Proc. R. Soc. Lond. Ser. B Biol. Sci.* **263**, 1033–1039 (1996).
28. Wiuf, C., Zhao, K., Innan, H. & Nordborg, M. The probability and chromosomal extent of *trans*-specific polymorphism. *Genetics* **168**, 2363–2372 (2004).
29. Seidel, H. S., Rockman, M. V. & Kruglyak, L. Widespread genetic incompatibility in *C. elegans* maintained by balancing selection. *Science* **319**, 589–594 (2008).
30. Greene, J. S. et al. Balancing selection shapes density-dependent foraging behaviour. *Nature* **539**, 254–258 (2016).
31. Van Sluijs, L. et al. Balancing selection shapes the intracellular pathogen response in natural *Caenorhabditis elegans* populations. Preprint at *bioRxiv* https://doi.org/10.1101/579151 (2019).
32. Thompson, O. A. et al. Remarkably divergent regions punctuate the genome assembly of the *Caenorhabditis elegans* Hawaiian strain CB4856. *Genetics* **200**, 975–989 (2015).
33. Kim, C. et al. Long-read sequencing reveals intra-species tolerance of substantial structural variations and new subtelomere formation in *C. elegans*. *Genome Res.* **29**, 1023–1035 (2019).
34. Richaud, A., Zhang, G., Lee, D., Lee, J. & Félix, M.-A. The local coexistence pattern of selfing genotypes in *Caenorhabditis elegans* natural metapopulations. *Genetics* **208**, 807–821 (2018).
35. Price, A. L. et al. Principal components analysis corrects for stratification in genome-wide association studies. *Nat. Genet.* **38**, 904–909 (2006).
36. Rockman, M. V. & Kruglyak, L. Recombinational landscape and population genomics of *Caenorhabditis elegans*. *PLoS Genet.* **5**, e1000419 (2009).
37. Rockman, M. V., Skrovanek, S. S. & Kruglyak, L. Selection at linked sites shapes heritable phenotypic variation in *C. elegans*. *Science* **330**, 372–376 (2010).
38. Cutter, A. D. & Payseur, B. A. Genomic signatures of selection at linked sites: unifying the disparity among species. *Nat. Rev. Genet.* **14**, 262–274 (2013).
39. Gimond, C. et al. Outbreeding depression with low genetic variation in selfing *Caenorhabditis nematodes*. *Evolution* **67**, 3087–3101 (2013).
40. Cutter, A. D., Morran, L. T. & Phillips, P. C. Males, outcrossing, and sexual selection in *Caenorhabditis* nematodes. *Genetics* **213**, 27–57 (2019).
41. Barrett, R. D. H. & Schluter, D. Adaptation from standing genetic variation. *Trends Ecol. Evol.* **23**, 38–44 (2008).
42. Schulenburg, H., Hoeppner, M. P., Weiner, J. 3rd & Bornberg-Bauer, E. Specificity of the innate immune system and diversity of C-type lectin domain (CTLD) proteins in the nematode *Caenorhabditis elegans*. *Immunobiology* **213**, 237–250 (2008).
43. Reddy, K. C. et al. An intracellular pathogen response pathway promotes proteostasis in *C. elegans*. *Curr. Biol.* **27**, 3544–3553.e5 (2017).
44. Bakowski, M. A. et al. Ubiquitin-mediated response to microsporidia and virus infection in *C. elegans*. *PLoS Pathog.* **10**, e1004200 (2014).
45. Chang, H. C., Paek, J. & Kim, D. H. Natural polymorphisms in *C. elegans* HECW-1 E3 ligase affect pathogen avoidance behaviour. *Nature* **480**, 525–529 (2011).
46. Troemel, E. R., Félix, M.-A., Whiteman, N. K., Barrière, A. & Ausubel, F. M. Microsporidia are natural intracellular parasites of the nematode *Caenorhabditis elegans*. *PLoS Biol.* **6**, 2736–2752 (2008).
47. Félix, M.-A. et al. Natural and experimental infection of *Caenorhabditis* nematodes by novel viruses related to nodaviruses. *PLoS Biol.* **9**, e1000586 (2011).
48. Chen, K., Franz, C. J., Jiang, H., Jiang, Y. & Wang, D. An evolutionarily conserved transcriptional response to viral infection in *Caenorhabditis* nematodes. *BMC Genom.* **18**, 303 (2017).
49. Balla, K. M., Andersen, E. C., Kruglyak, L. & Troemel, E. R. A wild *C. elegans* strain has enhanced epithelial immunity to a natural microsporidian parasite. *PLoS Pathog.* **11**, e1004583 (2015).

50. Ashe, A. et al. A deletion polymorphism in the *Caenorhabditis elegans* RIG-I homolog disables viral RNA dicing and antiviral immunity. *eLife* **2**, e00994 (2013).
51. Martin, N., Singh, J. & Aballay, A. Natural genetic variation in the *Caenorhabditis elegans* response to *Pseudomonas aeruginosa*. *G3* **7**, 1137–1147 (2017).
52. Thomas, C. G. et al. Full-genome evolutionary histories of selfing, splitting, and selection in *Caenorhabditis*. *Genome Res.* **25**, 667–678 (2015).
53. Kiontke, K. C. et al. A phylogeny and molecular barcodes for *Caenorhabditis*, with numerous new species from rotting fruits. *BMC Evol. Biol.* **11**, 339 (2011).
54. Busch, J. W. & Delph, L. F. Evolution: selfing takes species down Stebbins's blind alley. *Curr. Biol.* **27**, R61–R63 (2017).
55. Ferrari, C. et al. Ephemeral-habitat colonization and neotropical species richness of *Caenorhabditis* nematodes. *BMC Ecol.* **17**, 43 (2017).
56. Greene, J. S., Dobosiewicz, M., Butcher, R. A., McGrath, P. T. & Bargmann, C. I.Regulatory changes in two chemoreceptor genes contribute to a *Caenorhabditis elegans* QTL for foraging behavior. *eLife* **5**, e21454 (2016).
57. Lee, D. et al. Selection and gene flow shape niche-associated variation in pheromone response. *Nat. Ecol. Evol.* **3**, 1455–1463 (2019).
58. Webster, A. K. et al. Population selection and sequencing of *Caenorhabditis elegans* wild isolates identifies a region on chromosome III affecting starvation resistance. *G3* **9**, 3477–3488 (2019).
59. Ghosh, R., Andersen, E. C., Shapiro, J. A., Gerke, J. P. & Kruglyak, L. Natural variation in a chloride channel subunit confers avermectin resistance in *C. elegans*. *Science* **335**, 574–578 (2012).
60. Ben-David, E., Burga, A. & Kruglyak, L. A maternal-effect selfish genetic element in *Caenorhabditis elegans*. *Science* **356**, 1051–1055 (2017).
61. Liu, Y. et al. Pan-genome of wild and cultivated soybeans. *Cell* **182**, 162–176.e13 (2020).
62. Cutter, A. D., Wasmuth, J. D. & Washington, N. L. Patterns of molecular evolution in *Caenorhabditis* preclude ancient origins of selfing. *Genetics* **178**, 2093–2104 (2008).
63. Brandvain, Y., Slotte, T., Hazzouri, K. M., Wright, S. I. & Coop, G. Genomic identification of founding haplotypes reveals the history of the selfing species *Capsella rubella*. *PLoS Genet.* **9**, e1003754 (2013).
64. Todesco, M. et al. Massive haplotypes underlie ecotypic differentiation in sunflowers. *Nature* **584**, 602–607 (2020).
65. Burgarella, C. et al. Adaptive introgression: an untapped evolutionary mechanism for crop adaptation. *Front. Plant Sci.* **10**, 4 (2019).
66. Kanzaki, N. et al. Biology and genome of a newly discovered sibling species of *Caenorhabditis elegans*. *Nat. Commun.* **9**, 3216 (2018).
67. Andersen, E. C., Bloom, J. S., Gerke, J. P. & Kruglyak, L. A variant in the neuropeptide receptor *npr-1* is a major determinant of *Caenorhabditis elegans* growth and physiology. *PLoS Genet.* **10**, e1004156 (2014).
68. Cook, D. E., Zdraljevic, S., Roberts, J. P. & Andersen, E. C. CeNDR, the *Caenorhabditis elegans* Natural Diversity Resource. *Nucleic Acids Res.* **45**, D650–D657 (2017).
69. Cook, D. E. et al. The genetic basis of natural variation in *Caenorhabditis elegans* telomere length. *Genetics* **204**, 371–383 (2016).
70. Bolger, A. M., Lohse, M. & Usadel, B. Trimmomatic: a flexible trimmer for Illumina sequence data. *Bioinformatics* **30**, 2114–2120 (2014).
71. Li, H. A statistical framework for SNP calling, mutation discovery, association mapping and population genetical parameter estimation from sequencing data. *Bioinformatics* **27**, 2987–2993 (2011).
72. Li, H. & Durbin, R. Fast and accurate short read alignment with Burrows–Wheeler transform. *Bioinformatics* **25**, 1754–1760 (2009).
73. Li, H. Aligning sequence reads, clone sequences and assembly contigs with BWA-MEM. Preprint at https://arxiv.org/abs/1303.3997 (2013).
74. Lee, R. Y. N. et al. WormBase 2017: molting into a new stage. *Nucleic Acids Res.* **46**, D869–D874 (2018).
75. Poplin, R. et al. Scaling accurate genetic variant discovery to tens of thousands of samples. Preprint at *bioRxiv* https://doi.org/10.1101/201178 (2018).
76. Cingolani, P. et al. A program for annotating and predicting the effects of single nucleotide polymorphisms, SnpEff: SNPs in the genome of *Drosophila melanogaster* strain w^{1118}; *iso-2*; *iso-3*. *Fly* **6**, 80–92 (2012).
77. Ortiz, E. M. vcf2phylip v2.0: convert a VCF matrix into several matrix formats for phylogenetic analysis. *GitHub* https://github.com/edgardomortiz/vcf2phylip (2019).
78. Schliep, K. P. phangorn: phylogenetic analysis in R. *Bioinformatics* **27**, 592–593 (2011).
79. Yu, G., Smith, D. K., Zhu, H., Guan, Y. & Lam, T. T.-Y. ggtree: an R package for visualization and annotation of phylogenetic trees with their covariates and other associated data. *Methods Ecol. Evol.* **8**, 28–36 (2017).
80. Patterson, N., Price, A. L. & Reich, D. Population structure and eigenanalysis. *PLoS Genet.* **2**, e190 (2006).
81. Browning, B. L. & Browning, S. R. Detecting identity by descent and estimating genotype error rates in sequence data. *Am. J. Hum. Genet.* **93**, 840–851 (2013).
82. Miles, A., Ralph, P., Rae, S. & Pisupati, R. cggh/scikit-allel: v1.2.1. *Zenodo* https://doi.org/10.5281/zenodo.3238280 (2019).
83. Siewert, K. M. & Voight, B. F.BetaScan2: standardized statistics to detect balancing selection utilizing substitution data. *Genome Biol. Evol.* **12**, 3873–3877 (2020).
84. Siewert, K. BetaScan *GitHub* https://github.com/ksiewert/BetaScan (2017).
85. Zhang, C., Dong, S.-S., Xu, J.-Y., He, W.-M. & Yang, T.-L. PopLDdecay: a fast and effective tool for linkage disequilibrium decay analysis based on variant call format files. *Bioinformatics* **35**, 1786–1788 (2019).
86. Ruan, J. & Li, H. Fast and accurate long-read assembly with wtdbg2. *Nat. Methods* **17**, 155–158 (2020).
87. Kolmogorov, M., Yuan, J., Lin, Y. & Pevzner, P. A. Assembly of long, error-prone reads using repeat graphs. *Nat. Biotechnol.* **37**, 540–546 (2019).
88. Koren, S. et al. Canu: scalable and accurate long-read assembly via adaptive *k*-mer weighting and repeat separation. *Genome Res.* **27**, 722–736 (2017).
89. Simão, F. A., Waterhouse, R. M., Ioannidis, P., Kriventseva, E. V. & Zdobnov, E. M. BUSCO: assessing genome assembly and annotation completeness with single-copy orthologs. *Bioinformatics* **31**, 3210–3212 (2015).
90. Walker, B. J. et al. Pilon: an integrated tool for comprehensive microbial variant detection and genome assembly improvement. *PLoS ONE* **9**, e112963 (2014).
91. Laetsch, D. R. & Blaxter, M. L. BlobTools: interrogation of genome assemblies. *F1000Res.* **6**, 1287 (2017).
92. Li, H. Minimap2: pairwise alignment for nucleotide sequences. *Bioinformatics* **34**, 3094–3100 (2018).
93. Li, H. et al. The Sequence Alignment/Map format and SAMtools. *Bioinformatics* **25**, 2078–2079 (2009).
94. Camacho, C. et al. BLAST+: architecture and applications. *BMC Bioinform.* **10**, 421 (2009).
95. Pundir, S., Martin, M. J. & O'Donovan, C. in *Protein Bioinformatics: From Protein Modifications and Networks to Proteomics* (eds Wu, C. H. et al.) 41–55 (Springer, 2017).
96. Buchfink, B., Xie, C. & Huson, D. H. Fast and sensitive protein alignment using DIAMOND. *Nat. Methods* **12**, 59–60 (2015).
97. Quinlan, A. R. & Hall, I. M. BEDTools: a flexible suite of utilities for comparing genomic features. *Bioinformatics* **26**, 841–842 (2010).
98. Pedersen, B. S. & Quinlan, A. R. Mosdepth: quick coverage calculation for genomes and exomes. *Bioinformatics* **34**, 867–868 (2018).
99. *C. elegans* Sequencing Consortium. Genome sequence of the nematode *C. elegans*: a platform for investigating biology. *Science* **282**, 2012–2018 (1998).
100. Delcher, A. L., Salzberg, S. L. & Phillippy, A. M. Using MUMmer to identify similar regions in large sequence sets. *Curr. Protoc. Bioinform.* **10**, 10.3 (2003).
101. Robinson, J. T. et al. Integrative genomics viewer. *Nat. Biotechnol.* **29**, 24–26 (2011).
102. Holdorf, A. D. et al. WormCat: an online tool for annotation and visualization of *Caenorhabditis elegans* genome-scale data. *Genetics* **214**, 279–294 (2019).
103. Yu, G., Wang, L.-G., Han, Y. & He, Q.-Y. clusterProfiler: an R package for comparing biological themes among gene clusters. *OMICS* **16**, 284–287 (2012).
104. Carlson, M. org.Ce.eg.db: Genome wide annotation for Worm. R package version 3.8.2 https://bioconductor.org/packages/release/data/annotation/html/org.Ce.eg.db.html (2019).
105. Bao, W., Kojima, K. K. & Kohany, O. Repbase Update, a database of repetitive elements in eukaryotic genomes. *Mob. DNA* **6**, 11 (2015).
106. Stanke, M., Diekhans, M., Baertsch, R. & Haussler, D. Using native and syntenically mapped cDNA alignments to improve de novo gene finding. *Bioinformatics* **24**, 637–644 (2008).
107. Emms, D. M. & Kelly, S. OrthoFinder: solving fundamental biases in whole genome comparisons dramatically improves orthogroup inference accuracy. *Genome Biol.* **16**, 157 (2015).
108. Slater, G. S. C. & Birney, E. Automated generation of heuristics for biological sequence comparison. *BMC Bioinform.* **6**, 31 (2005).
109. Finn, R. D. et al. The Pfam protein families database: towards a more sustainable future. *Nucleic Acids Res.* **44**, D279–D285 (2016).
110. Jones, P. et al. InterProScan 5: genome-scale protein function classification. *Bioinformatics* **30**, 1236–1240 (2014).
111. Wickham, H. *ggplot2: Elegant Graphics for Data Analysis* (Springer, 2016).
112. Bradley, R. K. et al. Fast statistical alignment. *PLoS Comput. Biol.* **5**, e1000392 (2009).
113. Minh, B. Q. et al. IQ-TREE 2: new models and efficient methods for phylogenetic inference in the genomic era. *Mol. Biol. Evol.* **37**, 1530–1534 (2020).

114. Kalyaanamoorthy, S., Minh, B. Q., Wong, T. K. F., von Haeseler, A. & Jermiin, L. S. ModelFinder: fast model selection for accurate phylogenetic estimates. *Nat. Methods* **14**, 587–589 (2017).
115. Zheng, X. et al. A high-performance computing toolset for relatedness and principal component analysis of SNP data. *Bioinformatics* **28**, 3326–3328 (2012).
116. Stein, L. D. et al. The genome sequence of *Caenorhabditis briggsae*: a platform for comparative genomics. *PLoS Biol.* **1**, E45 (2003).
117. Yin, D. et al. Rapid genome shrinkage in a self-fertile nematode reveals sperm competition proteins. *Science* **359**, 55–61 (2018).
118. Stevens, L. et al. The genome of *Caenorhabditis bovis*. *Curr. Biol.* **30**, 1023–1031.e4 (2020).

Acknowledgements

We thank members of the Andersen laboratory for providing comments on this manuscript. We especially thank M. Ailion, J. David, R. Luallen, N. Pujol and citizen scientists for contributing wild *C. elegans* strains to CeNDR. We also thank the Duke University School of Medicine for use of the Sequencing and Genomic Technologies Shared Resource, which provided Pacific Biosciences long-read sequencing. This work was funded by an NSF CAREER award (1751035) and a Human Frontier Science Program Award (RGP0001/2019) (to E.C.A.). This work was also funded by National Institutes of Health (NIH) grant ES029930 (to E.C.A., M.V.R. and L.R.B.). S.Z. received funding from The Cellular and Molecular Basis of Disease training programme (T32GM008061) and the Rappaport Award for Research Excellence through the IBiS graduate programme. A.K.W. is supported by the National Science Foundation Graduate Research Fellowship. Long-read sequencing of three isolates was funded by the NIH (R01 GM117408 to L.R.B.) and a T32 training grant for the University Program in Genetics and Genomics (GM007754). M.V.R. is supported by NIH grant GM121828. M.G.S. was supported by an NWO Domain Applied and Engineering Sciences Veni grant (17282).

Author contributions

D.L., S.Z. and E.C.A. conceived of and designed the study. D.L., S.Z., L.S. and E.C.A. analysed the data and wrote the manuscript. Y.W., R.E.T. and D.E.C. performed whole-genome sequencing and isotype characterization for 609 wild *C. elegans* strains. R.E.T. performed long-read sequencing for 11 *C. elegans* wild isolates. R.C., A.K.W. and L.R.B. performed long-read sequencing for three *C. elegans* wild isolates. M.G.S., C.B., M.V.R. and M.-A.F. contributed wild isolates to the *C. elegans* strain collection. M.G.S., C.B., M.V.R., M.-A.F. and T.A.C. edited the manuscript.

Competing interests

The authors declare no competing interests.

Additional information

Extended data is available for this paper at https://doi.org/10.1038/s41559-021-01435-x.

Supplementary information The online version contains supplementary material available at https://doi.org/10.1038/s41559-021-01435-x.

Correspondence and requests for materials should be addressed to E.C.A.

Peer review information *Nature Ecology & Evolution* thanks the anonymous reviewers for their contribution to the peer review of this work. Peer reviewer reports are available.

Reprints and permissions information is available at www.nature.com/reprints.

Publisher's note Springer Nature remains neutral with regard to jurisdictional claims in published maps and institutional affiliations.

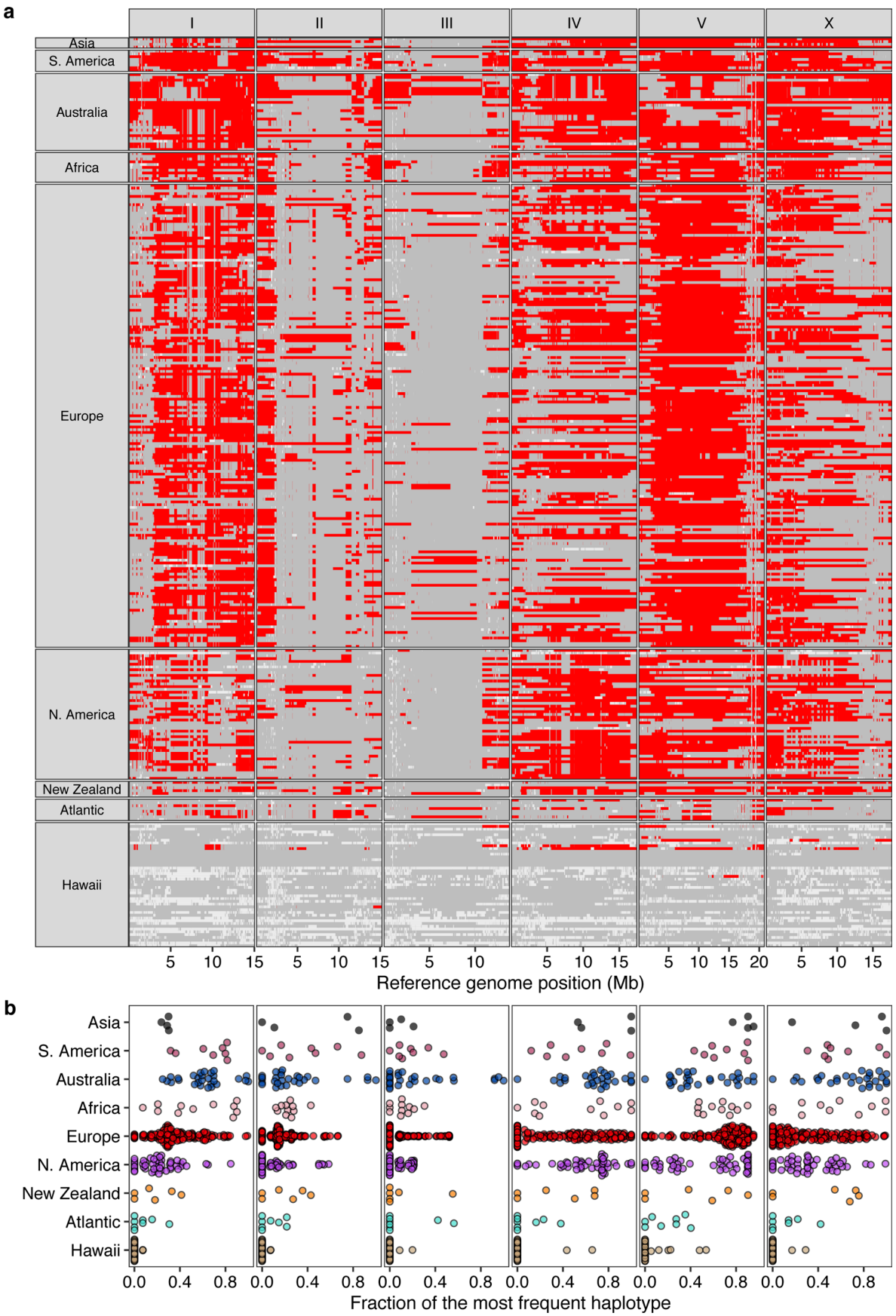

Extended Data Fig. 1 | See next page for caption.

Extended Data Fig. 1 | Chromosome-scale selective sweeps across wild *C. elegans* isotypes. a, The genome-wide distribution of the most frequent haplotype (red) among 324 wild isotypes with known geographic origin is shown. Grey genomic regions represent other haplotypes, and white represents unclassified haplotypes. Each row is one of the 324 isotypes, grouped by the geographic origin. The genomic position in Mb is plotted on the x-axis, and each tick mark represents 5 Mb of the chromosome. **b**, Beeswarm plots of the proportion of the most frequent haplotype for each chromosome from (a) for 324 isotypes with known geographic origins are shown. Wild isotypes are grouped by geographic origin. Each point corresponds to one of the 324 isotypes, and geographic origins are shown on the y-axis.

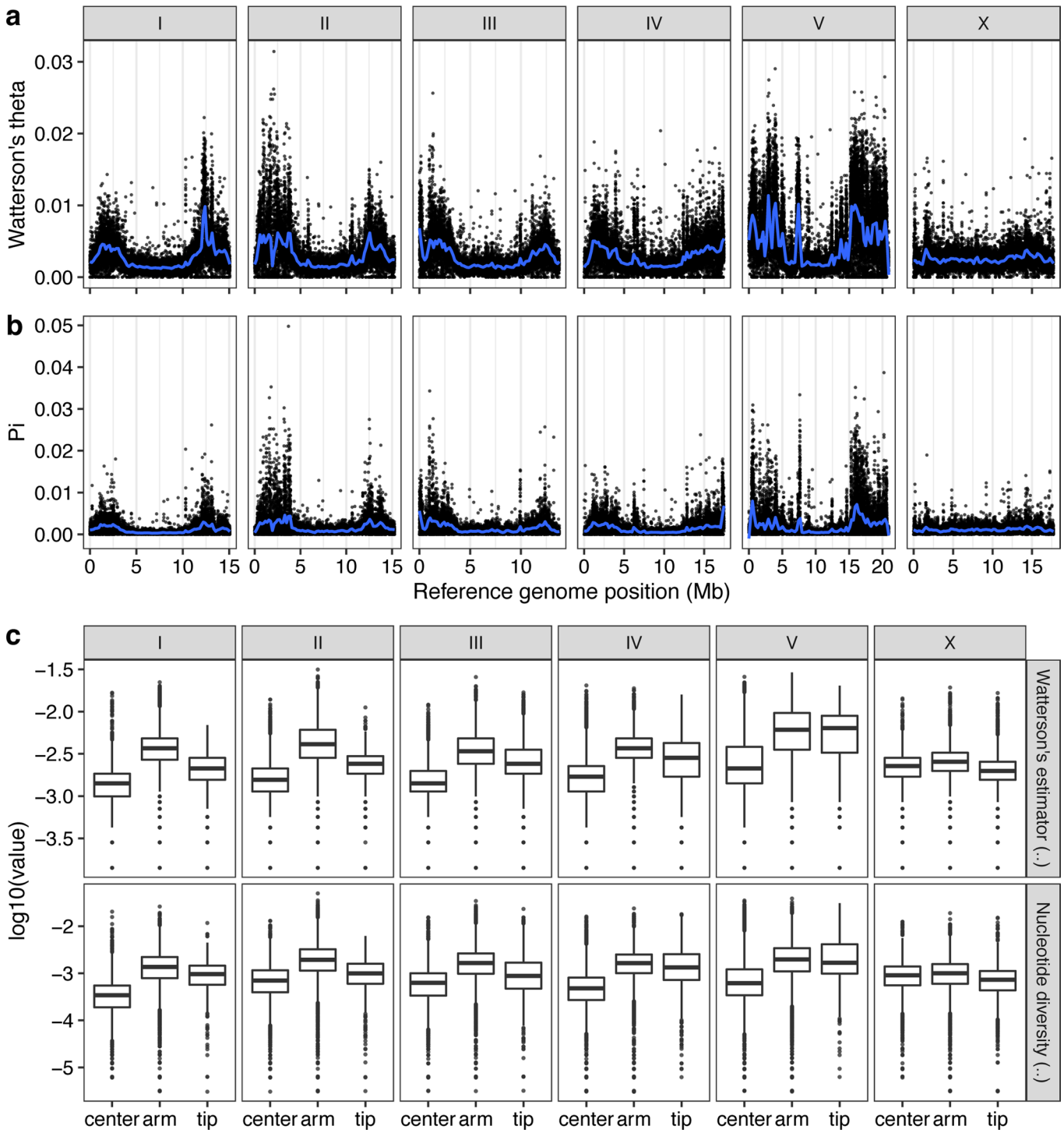

Extended Data Fig. 2 | Patterns of molecular diversity across the *C. elegans* genome. The chromosomal patterns **a**, Watterson's theta (θ) and **b**, nucleotide diversity (pi) for non-overlapping 1 kb windows are shown. Each dot corresponds to the calculated value for a particular window. The genomic position in Mb is plotted on the x-axis. Diversity statistic values are shown on the y-axis. Smoothed lines (blue) are LOESS fits. **c**, Tukey box plots of genetic diversity statistics from (**a**) are shown with outlier data points plotted. Genetic diversity statistics for each sliding window are grouped by the chromosomal region defined previously[36]. Genetic diversity statistic values are shown on the y-axis. The horizontal line in the middle of the box is the median, and the box denotes the 25th to 75th quantiles of the data. The vertical line represents the 1.5x interquartile range.

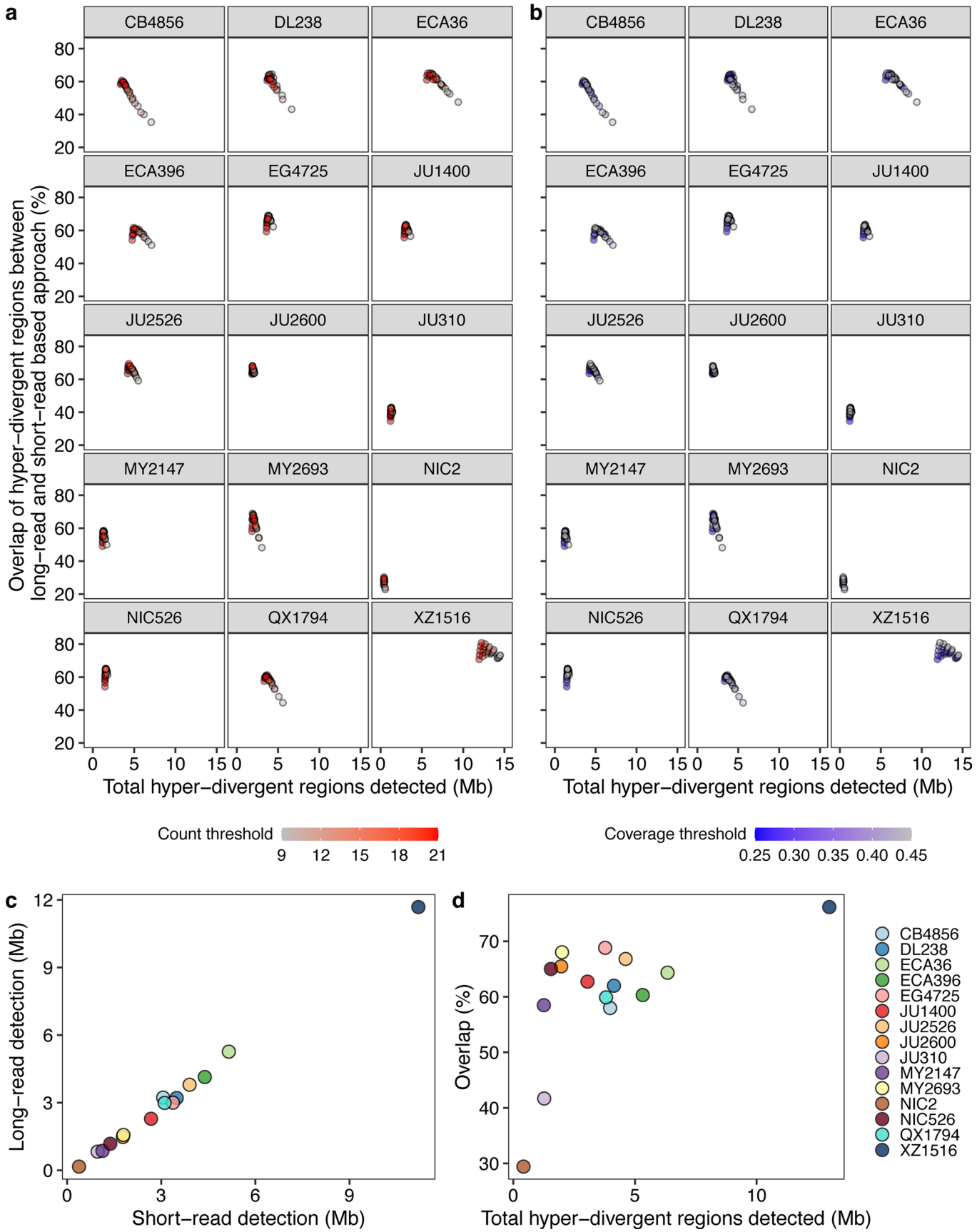

Extended Data Fig. 3 | See next page for caption.

Extended Data Fig. 3 | Optimization of parameters for the characterization of hyper-divergent regions. a,**b**, The total detected hyper-divergent regions in Mb (x-axis) and the percent overlap of long-read and short-read hyper-divergent classification (y-axis) are shown (Methods). Each point corresponds to one of the combination of threshold parameters for the variant count and coverage fraction of 1 kb bin to be classified as hyper-divergent. Each point is coloured by the variant count threshold (**a**) or the coverage fraction threshold (**b**). **c**, The relationship between the total size of hyper-divergent regions detected by the optimized short-read or long-read based approach is shown. Each point corresponds to one of the 15 long-read sequenced isotypes. Total sizes of hyper-divergent regions detected by the short-read based approach are shown on the x-axis, and total sizes of hyper-divergent regions detected by the long-read based approach are shown on the y-axis. **d**, The overlap between hyper-divergent regions defined by the optimized short-read based approach and long-read based approach is shown. Each point corresponds to one of the 15 long-read sequenced isotypes. Total sizes of hyper-divergent regions detected by either short-read or long-read based approach are shown on the x-axis, and the percentages of hyper-divergent regions detected by both approaches are shown on the y-axis.

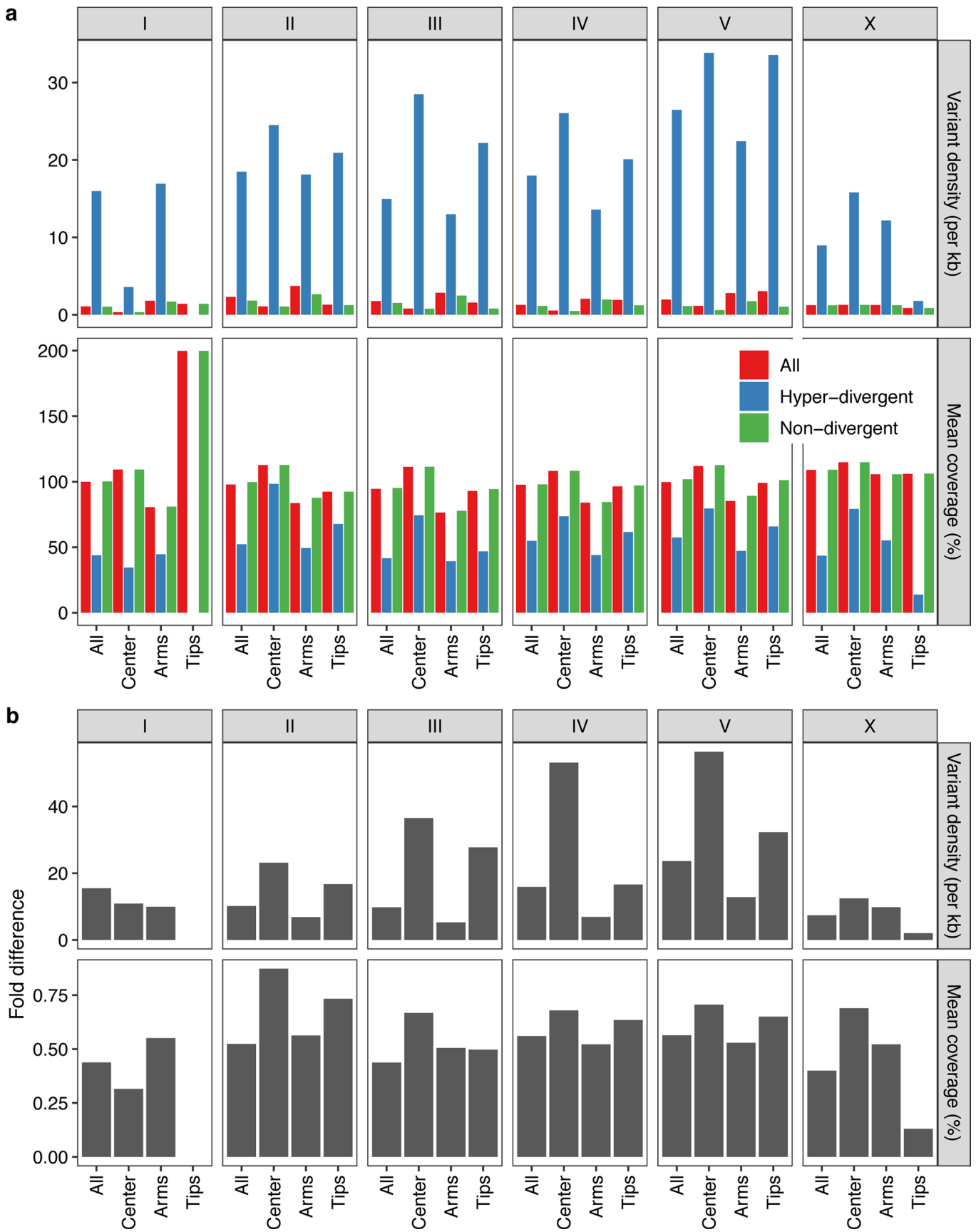

Extended Data Fig. 4 | See next page for caption.

Extended Data Fig. 4 | Summary statistics for hyper-divergent regions across six chromosomes. a, Bar plots for the comparisons of variant (SNV/indel) density (top) and coverage fraction (bottom) between hyper-divergent regions (red) and the rest of the regions (blue) in each chromosomal region are shown. Note that no hyper-divergent region was found on the tips of chromosome I. **b**, Fold differences between hyper-divergent regions and the rest of the regions from (**a**) are shown.

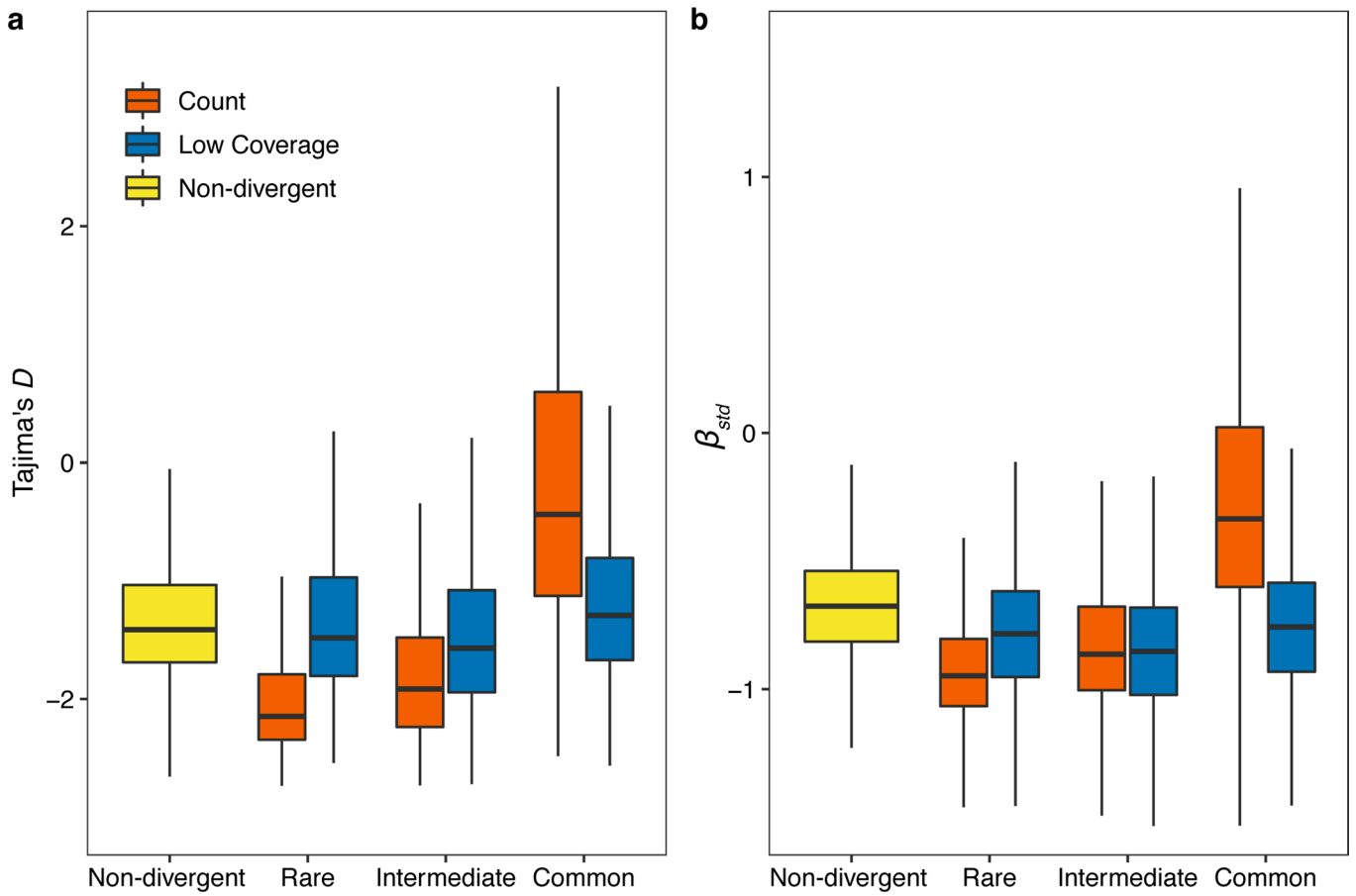

Extended Data Fig. 5 | Genomic signatures of balancing selection in non-divergent regions and hyper-divergent regions. Tukey box plots of Tajima's *D* (**a**) and standardized beta (**b**) are shown. Genomic bins (1 kb) (**a**) or variants (**b**) are grouped and coloured by their classification: (1) non-divergent bins (yellow), (2) hyper-divergent bins with high variant density (≥ 16 SNVs/indels, red), (3) hyper-divergent bins with low read depth (< 35%, blue). Hyper-divergent bins are grouped by their species-wide frequencies: rare (<1%), intermediate (≥ 1% and < 5%), or common (≥ 5%). The horizontal line in the middle of the box is the median, and the box denotes the 25th to 75th quantiles of the data. The vertical line represents the 1.5x interquartile range.

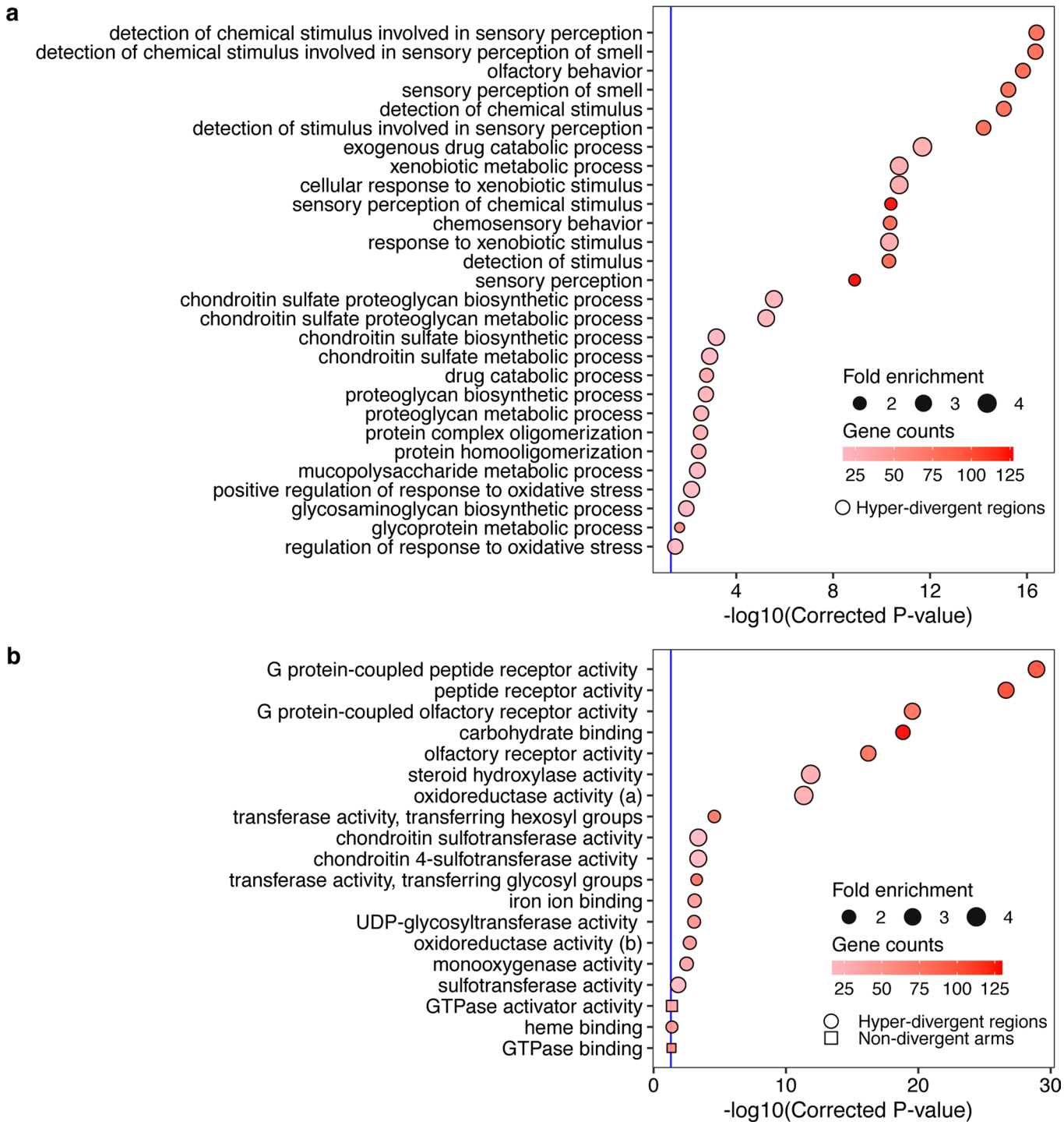

Extended Data Fig. 6 | Gene ontology (GO) enrichment for hyper-divergent regions. Gene ontology (GO) enrichment for the biological process category (**a**) and the molecular function category (**b**) for non-divergent chromosomal arms (square) and hyper-divergent regions (circle) are shown. Significantly enriched GO terms in control regions or hyper-divergent regions or both are shown on the y-axis. Bonferroni-corrected significance values for GO enrichment are shown on the x-axis. Sizes of squares and circles correspond to the fold enrichment of the annotation, and colours of square and circle correspond to the gene counts of the annotation. The blue line shows the Bonferroni-corrected significance threshold (corrected p-value = 0.05). Note, we did not detect any GO-term enrichment of genes in non-divergent chromosomal arms for the biological process category.

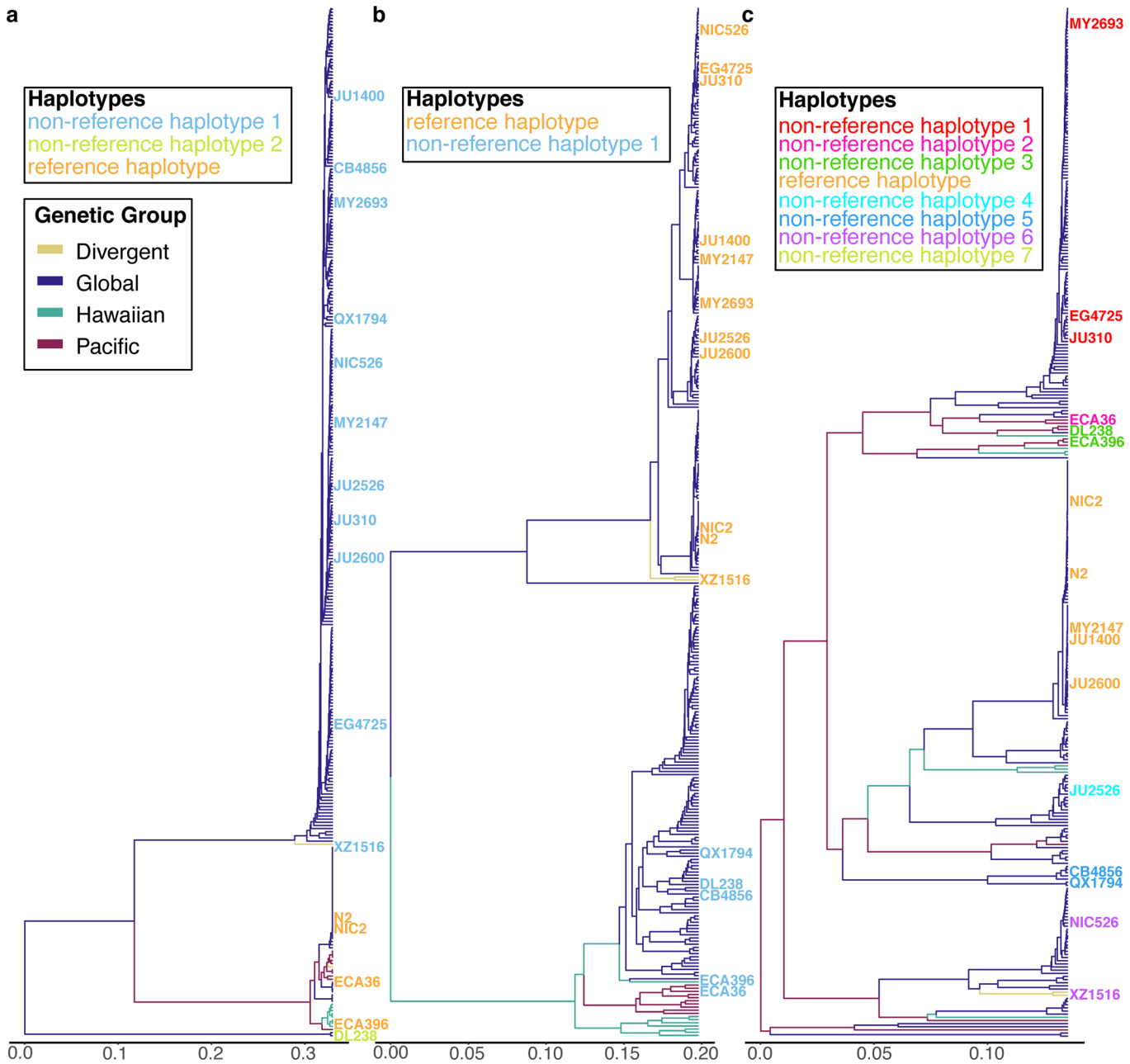

Extended Data Fig. 7 | Species-wide SNP-based relatedness of divergent regions is in agreement with long-read sequencing results. The inferred for the *C. elegans* species-wide relatedness for the hyper-divergent regions that span (**a**) II:3,667,179-3,701,405, (**b**) I:2,318,291-2,381,851, and (**c**) V:20,193,463-20,267,244 are shown. The x-axis represents the dissimilarity of the fraction of identity-by-state in the region. For a-c, the isotype names are coloured to match the haplotypes defined by long-read sequence data in Fig. 5 and Extended Data Figs. 8, 9, respectively. The branch colours correspond to the species-wide genetic groups identified by PCA in Fig. 1c.

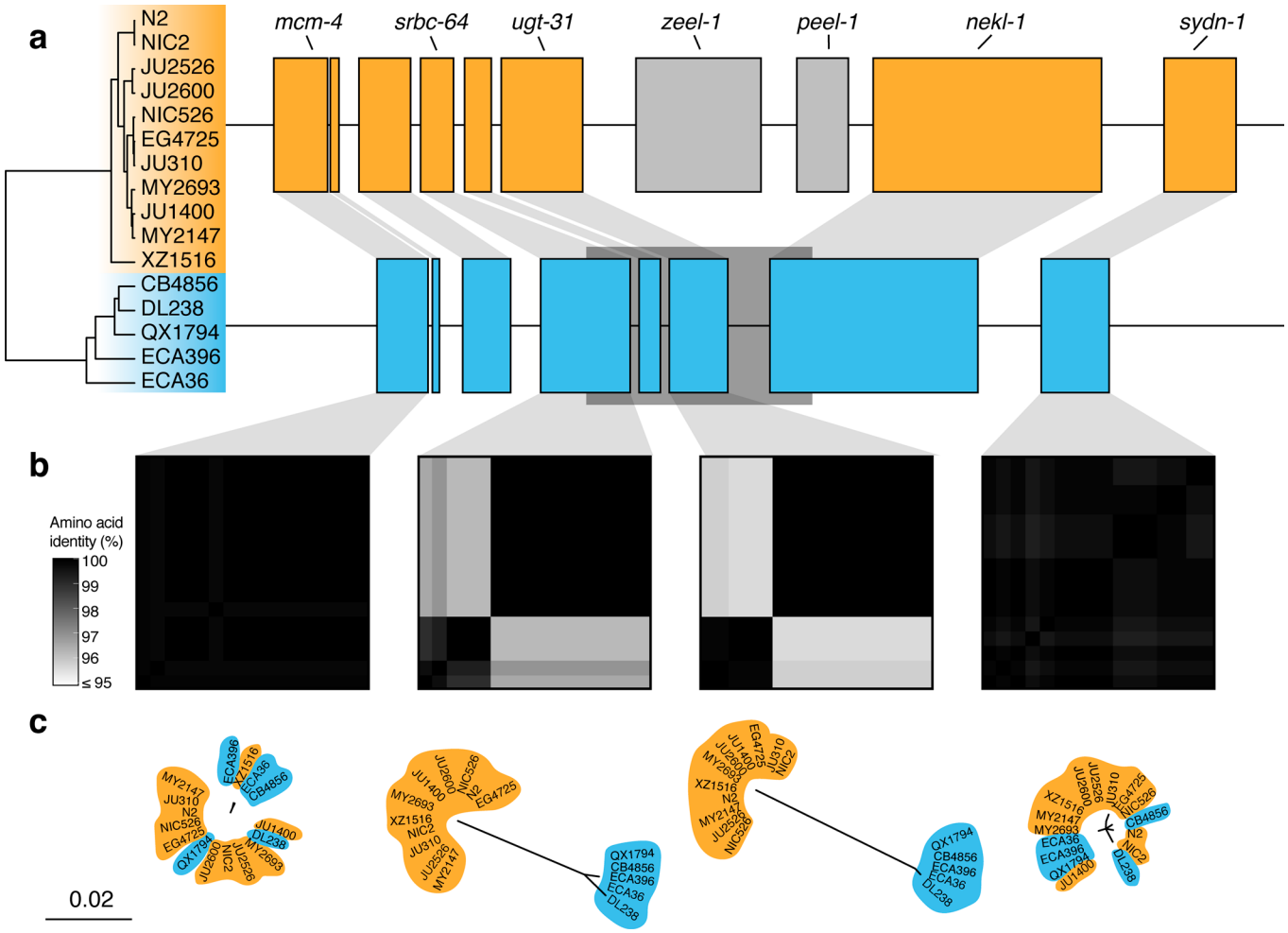

Extended Data Fig. 8 | Two hyper-divergent haplotypes at the *peel-1 zeel-1* incompatibility locus. a, The protein-coding gene contents of the two hyper-divergent haplotypes at the *peel-1 zeel-1* incompatibility locus on the left arm of chromosome I (I:2,318,291-2,381,851 of the N2 reference genome). The tree was inferred using SNVs and coloured by inferred haplotypes. For each distinct haplotype, we chose a single isotype as a haplotype representative (orange haplotype: N2, blue haplotype: CB4856) and predicted protein-coding genes using both protein-based alignments and *ab initio* approaches. Protein-coding genes are shown as boxes; those genes that are conserved in all haplotypes are coloured based on their haplotype, and those genes that are not are coloured light grey. Dark grey boxes behind genes indicate coordinates of divergent regions. Genes with locus names in N2 are highlighted. **b**, Heatmaps showing amino acid identity for alleles of four genes (*mcm-4*, *srbc-64*, *ugt-31*, and *sydn-1*). The percentage identity was calculated using alignments of protein sequences from all 16 isotypes. Heatmaps are ordered by the SNV tree shown in (**a**). **c**, Maximum-likelihood gene trees of four genes (*mcm-4*, *srbc-64*, *ugt-31*, and *sydn-1*) inferred using amino acid alignments. Trees are plotted on the same scale (scale shown; scale is in substitutions per site). Strain names are coloured by their haplotype.

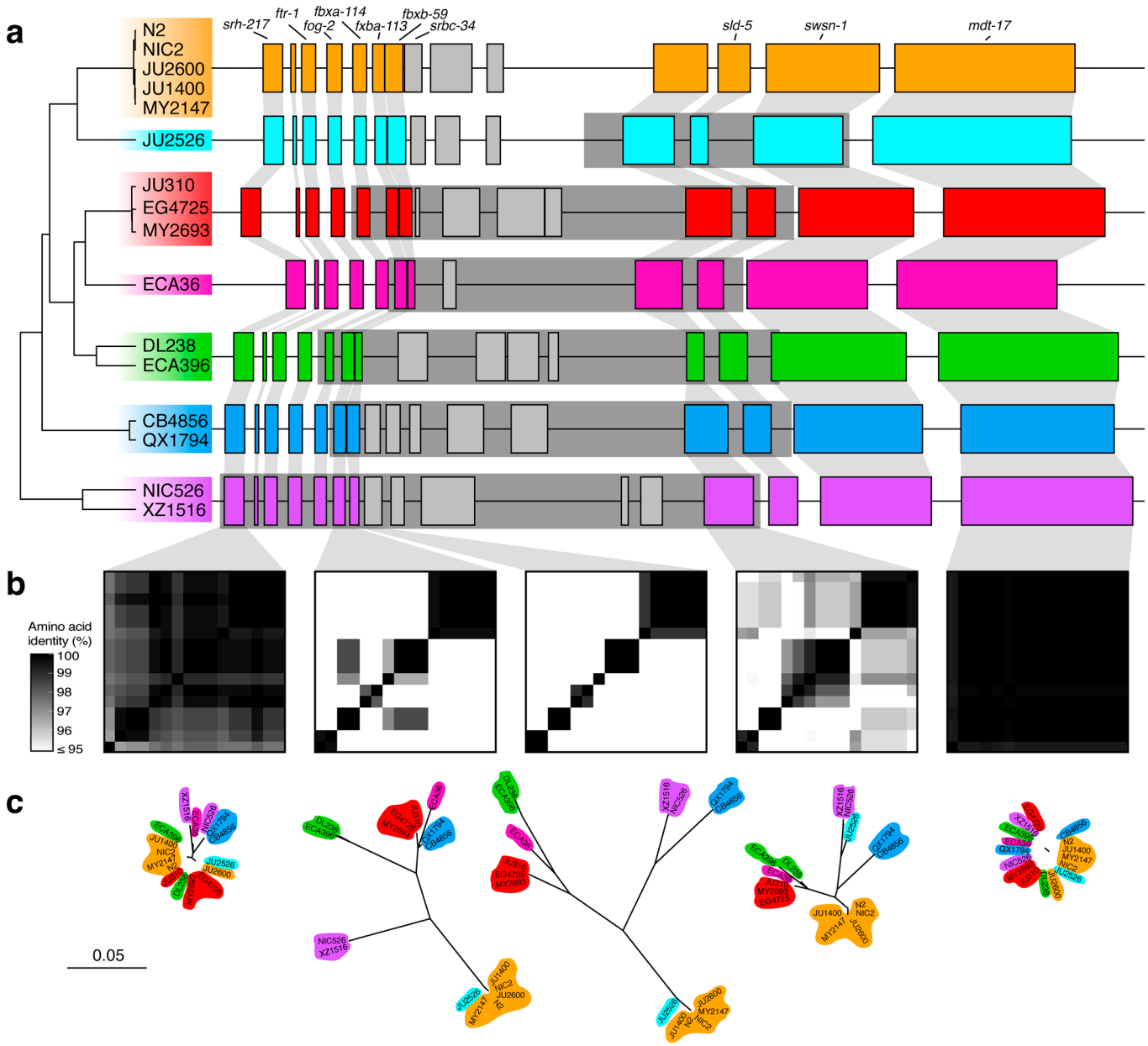

Extended Data Fig. 9 | Hyper-divergent haplotypes at a region on the right arm of chromosome V. a, The protein-coding gene contents of the seven hyper-divergent haplotypes at a region on the right arm of chromosome V (V:20,193,463-20,267,244 of the N2 reference genome). The tree was inferred using SNVs and coloured by inferred haplotypes. For each distinct haplotype, we chose a single isotype as a haplotype representative (orange haplotype: N2, light blue haplotype: JU2526, red haplotype: EG4725, pink haplotype: ECA36, green haplotype: DL238, dark blue haplotype: QX1794, purple haplotype: NIC526) and predicted protein-coding genes using both protein-based alignments and *ab initio* approaches. JU2526 shares the reference haplotype at *fbxa-113* and *fbxb-59* (six hyper-divergent haplotypes at these loci) but is divergent at *Y113G7B.15* (seven hyper-divergent haplotypes at this locus). Protein-coding genes are shown as boxes; those genes that are conserved in all haplotypes are coloured based on their haplotypes, and those genes that are not are coloured light grey. Dark grey boxes behind genes indicate coordinates of divergent regions. Genes with locus names in N2 are highlighted. Of the 25 genes that are not conserved in all haplotypes (light grey boxes), ten are alleles of the three reference haplotype (N2) loci coloured in light grey. The remaining 15 do not have a clear one-to-one relationship with a gene in the reference haplotype. Seven of these 15 have homology to *F54E12.2* (present in the reference haplotype) and are likely the product of duplication and diversification. Six have homology to either *M04C3.1, F19B2.5*, or *F54E12.2*, all of which are genes with SNF2 family N-terminal domains and which exist elsewhere in the N2 reference genome. Of the remaining two genes, one has homology to *Y113G7B.15*, which is present in the reference haplotype, and the other has homology to *W09C3.8*, a gene on chromosome I in the reference genome. Functional annotations of all unconserved loci (including BLAST hits and Pfam domains identified by InterProScan) can be found in Supplementary Data 4. **b**, Heatmaps show amino acid identity for between alleles of five genes (*srh-217*, *fbxb-113*, *fbxb-59*, *Y113G7B.15*, and *mdt-17*). The percentage identity was calculated using alignments of proteins sequences from all 16 isotypes. Heatmaps are ordered by the SNV tree shown in (**a**). **c**, Maximum-likelihood gene trees of five genes (*srh-217*, *fbxb-113*, *fbxb-59*, *Y113G7B.15*, and *mdt-17*) inferred using amino acid alignments. Trees are plotted on the same scale (scale shown; scale is in substitutions per site). Strain names are coloured by their haplotype.

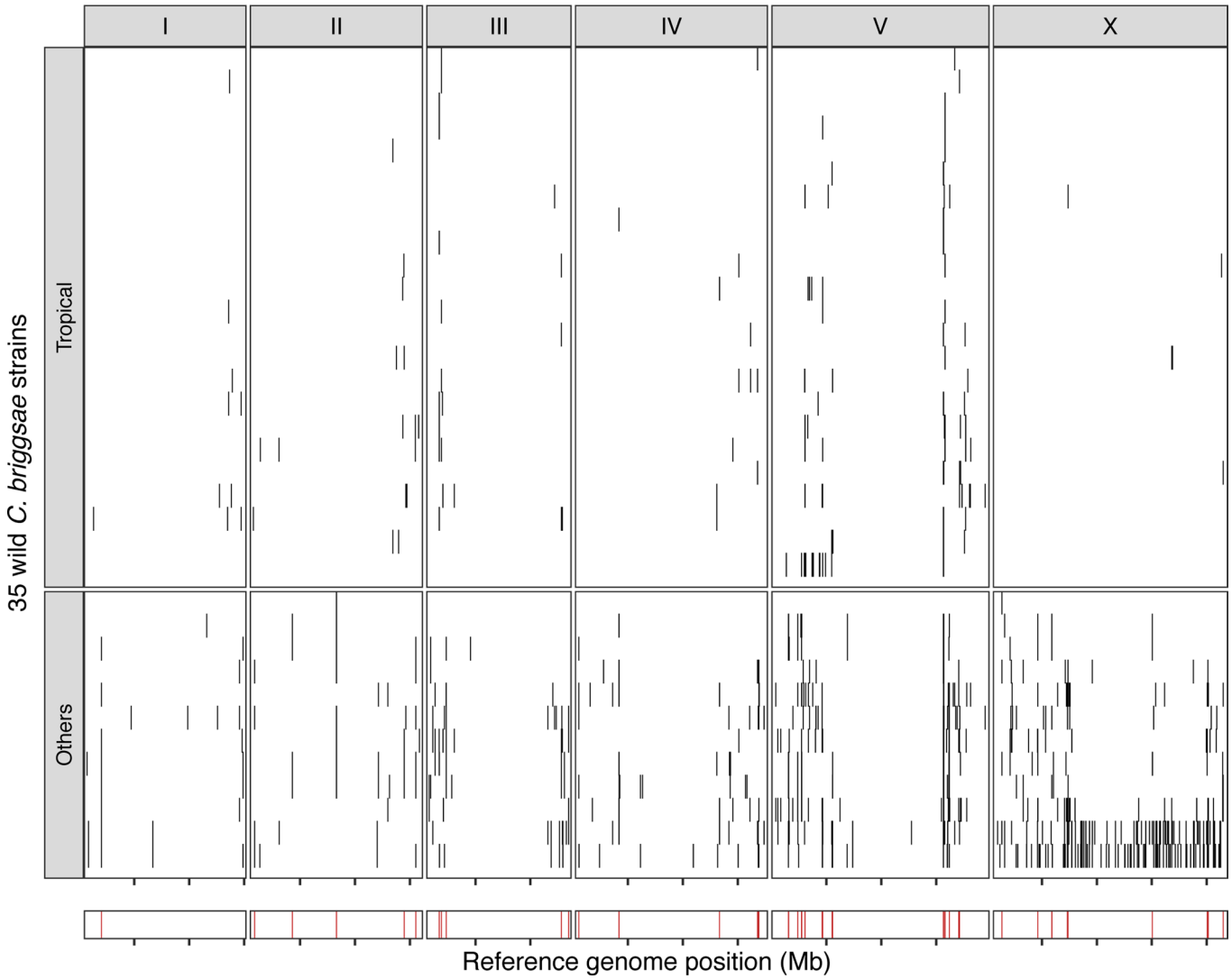

Extended Data Fig. 10 | Hyper-divergent regions in *C. briggsae*. The genome-wide distribution of hyper-divergent regions across 35 non-reference wild *C. briggsae* strains is shown. In the top panel, each row is one of the 35 strains, grouped by previously defined clades (tropical or others) ordered by the total amount of genome covered by hyper-divergent regions (black). In the bottom panel, brown bars indicate genomic positions in which more than 10% of strains are classified as hyper-divergent at the locus. The genomic position in Mb is plotted on the x-axis, and each tick represents 5 Mb of the chromosome.

nature research

Corresponding author(s): Erik C. Andersen

Last updated by author(s): Feb 25, 2021

Reporting Summary

Nature Research wishes to improve the reproducibility of the work that we publish. This form provides structure for consistency and transparency in reporting. For further information on Nature Research policies, see our Editorial Policies and the Editorial Policy Checklist.

Statistics

For all statistical analyses, confirm that the following items are present in the figure legend, table legend, main text, or Methods section.

n/a	Confirmed	
☒	☐	The exact sample size (*n*) for each experimental group/condition, given as a discrete number and unit of measurement
☒	☐	A statement on whether measurements were taken from distinct samples or whether the same sample was measured repeatedly
☐	☒	The statistical test(s) used AND whether they are one- or two-sided *Only common tests should be described solely by name; describe more complex techniques in the Methods section.*
☐	☒	A description of all covariates tested
☐	☒	A description of any assumptions or corrections, such as tests of normality and adjustment for multiple comparisons
☐	☒	A full description of the statistical parameters including central tendency (e.g. means) or other basic estimates (e.g. regression coefficient) AND variation (e.g. standard deviation) or associated estimates of uncertainty (e.g. confidence intervals)
☒	☐	For null hypothesis testing, the test statistic (e.g. *F*, *t*, *r*) with confidence intervals, effect sizes, degrees of freedom and *P* value noted *Give P values as exact values whenever suitable.*
☒	☐	For Bayesian analysis, information on the choice of priors and Markov chain Monte Carlo settings
☒	☐	For hierarchical and complex designs, identification of the appropriate level for tests and full reporting of outcomes
☒	☐	Estimates of effect sizes (e.g. Cohen's *d*, Pearson's *r*), indicating how they were calculated

Our web collection on statistics for biologists contains articles on many of the points above.

Software and code

Policy information about availability of computer code

Data collection: No software was used for data collection.

Data analysis:

1. Bolger, A. M., Lohse, M. & Usadel, B. Trimmomatic: a flexible trimmer for Illumina sequence data. Bioinformatics 30, 2114–2120 (2014).
2. Li, H. A statistical framework for SNP calling, mutation discovery, association mapping and population genetical parameter estimation from sequencing data. Bioinformatics 27, 2987–2993 (2011).
3. Poplin, R. et al. Scaling accurate genetic variant discovery to tens of thousands of samples. bioRxiv 201178 (2018) doi:10.1101/201178.
4.. Cingolani, P. et al. A program for annotating and predicting the effects of single nucleotide polymorphisms, SnpEff: SNPs in the genome of Drosophila melanogaster strain w1118; iso-2; iso-3. Fly 6, 80–92 (2012).
5. Ortiz, E. M. vcf2phylip. (Github).
6.. Schliep, K. P. phangorn: phylogenetic analysis in R. Bioinformatics 27, 592–593 (2011).
7.. Yu, G., Smith, D. K., Zhu, H., Guan, Y. & Lam, T. T.-Y. ggtree : an r package for visualization and annotation of phylogenetic trees with their covariates and other associated data. Methods Ecol. Evol. 8, 28–36 (2017).
8. Patterson, N., Price, A. L. & Reich, D. Population structure and eigenanalysis. PLoS Genet. 2, e190 (2006).
9. Browning, B. L. & Browning, S. R. Detecting identity by descent and estimating genotype error rates in sequence data. Am. J. Hum. Genet. 93, 840–851 (2013).
10. Miles, A., Ralph, P., Rae, S. & Pisupati, R. cggh/scikit-allel: v1.2.1. (2019). doi:10.5281/zenodo.3238280.
11. Zhang, C., Dong, S.-S., Xu, J.-Y., He, W.-M. & Yang, T.-L. PopLDdecay: a fast and effective tool for linkage disequilibrium decay analysis based on variant call format files. Bioinformatics 35, 1786–1788 (2019).
12. Quinlan, A. R. & Hall, I. M. BEDTools: a flexible suite of utilities for comparing genomic features. Bioinformatics 26, 841–842 (2010).
13. Pedersen, B. S. & Quinlan, A. R. Mosdepth: quick coverage calculation for genomes and exomes. Bioinformatics 34, 867–868 (2018).
14. Holdorf, A. D. et al. WormCat: An Online Tool for Annotation and Visualization of Caenorhabditis elegans Genome-Scale Data. Genetics (2019) doi:10.1534/genetics.119.302919.
15. Yu, G., Wang, L.-G., Han, Y. & He, Q.-Y. clusterProfiler: an R package for comparing biological themes among gene clusters. OMICS 16, 284–

287 (2012).
16. Carlson, M. org.Ce.eg.db: Genome wide annotation for Worm. R package version 3.8.2. Bioconductor https://bioconductor.org/packages/release/data/annotation/html/org.Ce.eg.db.html (2019).
17. Andersen, E. C. et al. A Powerful New Quantitative Genetics Platform, Combining Caenorhabditis elegans High-Throughput Fitness Assays with a Large Collection of Recombinant Strains. G3 5, g3.115.017178–920 (2015).
18. Shimko, T. C. & Andersen, E. C. COPASutils: an R package for reading, processing, and visualizing data from COPAS large-particle flow cytometers. PLoS One 9, e111090 (2014).
19. easysorter. (Github).
20. Endelman, J. B. Ridge Regression and Other Kernels for Genomic Selection with R Package rrBLUP. The Plant Genome Journal 4, 250–256 (2011).
21. Qiu, Y. RSpectra. (Github).
22. Bilgrau, A. E. correlateR. (Github, 2018).
23. Riemondy, K. A. et al. valr: Reproducible genome interval analysis in R. F1000Res. 6, 1025 (2017).
24. Ruan, J. & Li, H. Fast and accurate long-read assembly with wtdbg2. Nat. Methods 17, 155–158 (2020).
25. Koren, S. et al. Canu: scalable and accurate long-read assembly via adaptive k-mer weighting and repeat separation. Genome Res. 27, 722–736 (2017).
26. Simão, F. A., Waterhouse, R. M., Ioannidis, P., Kriventseva, E. V. & Zdobnov, E. M. BUSCO: assessing genome assembly and annotation completeness with single-copy orthologs. Bioinformatics 31, 3210–3212 (2015).
27. Li, H. Aligning sequence reads, clone sequences and assembly contigs with BWA-MEM. arXiv [q-bio.GN] (2013).
28. Walker, B. J. et al. Pilon: an integrated tool for comprehensive microbial variant detection and genome assembly improvement. PLoS One 9, e112963 (2014).
29. Laetsch, D. R. & Blaxter, M. L. BlobTools: Interrogation of genome assemblies. F1000Res. 6, 1287 (2017).
30. Li, H. Minimap2: pairwise alignment for nucleotide sequences. Bioinformatics 34, 3094–3100 (2018).
31. Li, H. et al. The Sequence Alignment/Map format and SAMtools. Bioinformatics 25, 2078–2079 (2009).
32. Camacho, C. et al. BLAST+: architecture and applications. BMC Bioinformatics 10, 421 (2009).
33. Pundir, S., Martin, M. J. & O'Donovan, C. UniProt Protein Knowledgebase. in Protein Bioinformatics: From Protein Modifications and Networks to Proteomics (eds. Wu, C. H., Arighi, C. N. & Ross, K. E.) 41–55 (Springer New York, 2017).
34. Buchfink, B., Xie, C. & Huson, D. H. Fast and sensitive protein alignment using DIAMOND. Nat. Methods 12, 59–60 (2015).
35. R., S. A. H. RepeatMasker. http://www.repeatmasker.org (2008-2015).
36. Bao, W., Kojima, K. K. & Kohany, O. Repbase Update, a database of repetitive elements in eukaryotic genomes. Mob. DNA 6, 11 (2015).
37. Delcher, A. L., Salzberg, S. L. & Phillippy, A. M. Using MUMmer to identify similar regions in large sequence sets. Curr. Protoc. Bioinformatics Chapter 10, Unit 10.3 (2003).
38. Emms, D. M. & Kelly, S. OrthoFinder: solving fundamental biases in whole genome comparisons dramatically improves orthogroup inference accuracy. Genome Biol. 16, 157 (2015).
39. Finn, R. D. et al. The Pfam protein families database: towards a more sustainable future. Nucleic Acids Res. 44, D279–85 (2016).
40. Jones, P. et al. InterProScan 5: genome-scale protein function classification. Bioinformatics 30, 1236–1240 (2014).
41. Wickham, H. ggplot2: elegant graphics for data analysis. (2016).
42. Bradley, R. K. et al. Fast statistical alignment. PLoS Comput. Biol. 5, e1000392 (2009).
43. Minh, B. Q. et al. IQ-TREE 2: New Models and Efficient Methods for Phylogenetic Inference in the Genomic Era. Mol. Biol. Evol. 37, 1530–1534 (2020).
44. Kalyaanamoorthy, S., Minh, B. Q., Wong, T. K. F., von Haeseler, A. & Jermiin, L. S. ModelFinder: fast model selection for accurate phylogenetic estimates. Nat. Methods 14, 587–589 (2017).
45. Zheng, X. et al. A high-performance computing toolset for relatedness and principal component analysis of SNP data. Bioinformatics 28, 3326–3328 (2012).

For manuscripts utilizing custom algorithms or software that are central to the research but not yet described in published literature, software must be made available to editors and reviewers. We strongly encourage code deposition in a community repository (e.g. GitHub). See the Nature Research guidelines for submitting code & software for further information.

Data

Policy information about availability of data

All manuscripts must include a data availability statement. This statement should provide the following information, where applicable:

- Accession codes, unique identifiers, or web links for publicly available datasets
- A list of figures that have associated raw data
- A description of any restrictions on data availability

The raw sequencing reads for strains used in this project are available from the NCBI Sequence Read Archive (Project PRJNA549503).
The raw sequencing reads for strains used in this project are available from the NCBI Sequence Read Archive (Project PRJNA647911).
All data sets and code for generating figures and tables are available on GitHub (https://github.com/AndersenLab/Ce-328pop-div).

Field-specific reporting

Please select the one below that is the best fit for your research. If you are not sure, read the appropriate sections before making your selection.

☒ Life sciences ☐ Behavioural & social sciences ☐ Ecological, evolutionary & environmental sciences

For a reference copy of the document with all sections, see nature.com/documents/nr-reporting-summary-flat.pdf

Life sciences study design

All studies must disclose on these points even when the disclosure is negative.

Sample size	NA
Data exclusions	No data were excluded
Replication	NA
Randomization	NA
Blinding	NA

Reporting for specific materials, systems and methods

We require information from authors about some types of materials, experimental systems and methods used in many studies. Here, indicate whether each material, system or method listed is relevant to your study. If you are not sure if a list item applies to your research, read the appropriate section before selecting a response.

Materials & experimental systems

n/a	Involved in the study
☒	☐ Antibodies
☒	☐ Eukaryotic cell lines
☒	☐ Palaeontology and archaeology
☐	☒ Animals and other organisms
☒	☐ Human research participants
☒	☐ Clinical data
☒	☐ Dual use research of concern

Methods

n/a	Involved in the study
☒	☐ ChIP-seq
☒	☐ Flow cytometry
☒	☐ MRI-based neuroimaging

Animals and other organisms

Policy information about studies involving animals; ARRIVE guidelines recommended for reporting animal research

Laboratory animals	Caenorhabditis elegans
Wild animals	*Provide details on animals observed in or captured in the field; report species, sex and age where possible. Describe how animals were caught and transported and what happened to captive animals after the study (if killed, explain why and describe method; if released, say where and when) OR state that the study did not involve wild animals.*
Field-collected samples	*For laboratory work with field-collected samples, describe all relevant parameters such as housing, maintenance, temperature, photoperiod and end-of-experiment protocol OR state that the study did not involve samples collected from the field.*
Ethics oversight	*Identify the organization(s) that approved or provided guidance on the study protocol, OR state that no ethical approval or guidance was required and explain why not.*

Note that full information on the approval of the study protocol must also be provided in the manuscript.